Proton Imaging in Laser-Plasma Interactions

Andrea Macchi

polyLab, CNR-INFM
Dipartimento di Fisica "Enrico Fermi", Università di Pisa
Pisa, Italy

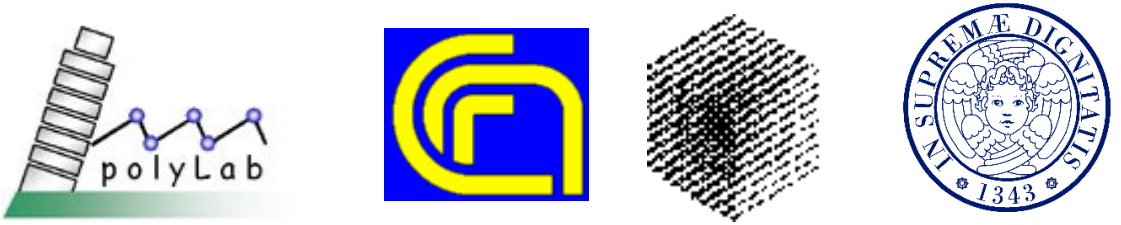

Bothe Kolloquium
Max-Planck-Institut fuer Kernphysik, Heidelberg

Wednesday, April 18, 2007

Coworkers (short list)

Alessandra Bigongiari, Francesco Ceccherini,
Fulvio Cornolti, Tatiana V. Liseykina,
Francesco Pegoraro

Dipartimento di Fisica "Enrico Fermi", Università di Pisa

Marco Borghesi, Satyabrata Kar, Lorenzo Romagnani

International Research Centre for Experimental Physics,
School of Mathematics and Physics,
Queen's University, Belfast, UK

Collaboration supported by a
Royal Society joint project

Coworkers (long list)

Alessandra Bigongiari, Francesco Ceccherini, Fulvio Cornolti, Tatiana V. Liseykina, Francesco Pegoraro *Dipartimento di Fisica "Enrico Fermi", Università di Pisa, Italy*

Marco Borghesi, Carlo Alberto Cecchetti, Satyabrata Kar, Lorenzo Romagnani
International Research Centre for Experimental Physics,
School of Mathematics and Physics, Queen's University, Belfast, UK

Angelo Schiavi *Università "La Sapienza" di Roma, Italy*

O. Willi, T. Toncian, R. Jung, J. Osterholz, G. Pretzler
Institut fuer Laser und Plasmaphysik, Heinrich-Heine-Universitaet,
Duesseldorf, Germany

J. Fuchs, P. Antici, P. Audebert *LULI, Ecole Polytechnique, Palaiseau, France*

P. Mora, T. Grismayer *LULI, Ecole Polytechnique, Palaiseau, France*

R. Heathcote, M. Galimberti
Central Laser Facility, Rutherford Appleton Laboratory, Chilton, UK

L. A. Gizzi *Intense Laser Irradiation Laboratory, IPCF-CNR, Pisa, Italy*

T. Cowan *Physics Department, University of Nevada, Reno, USA*

Outline

- The discovery of laser-accelerated protons
- “Proton Imaging”: how it works
- Investigations of laser-plasma phenomena based on “Proton Imaging”

The discovery of MeV protons in high-intensity laser interaction with solid targets (and some foreseen applications)

24 Centuries of Focused Light Interaction with Matter

Archimede, III century B.C.

Leonardo Da Vinci,
XVI century A.C.

Progress in focused laser intensity
across the XX and XXI centuries A.C.

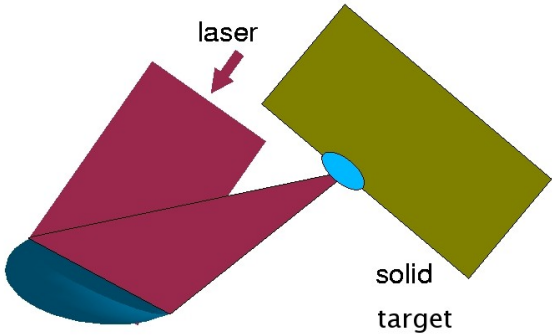

Highest intensity demonstrated:

10^{21} W/cm^2

(Center for Ultrafast Optical Science,
University of Michigan, 2005)

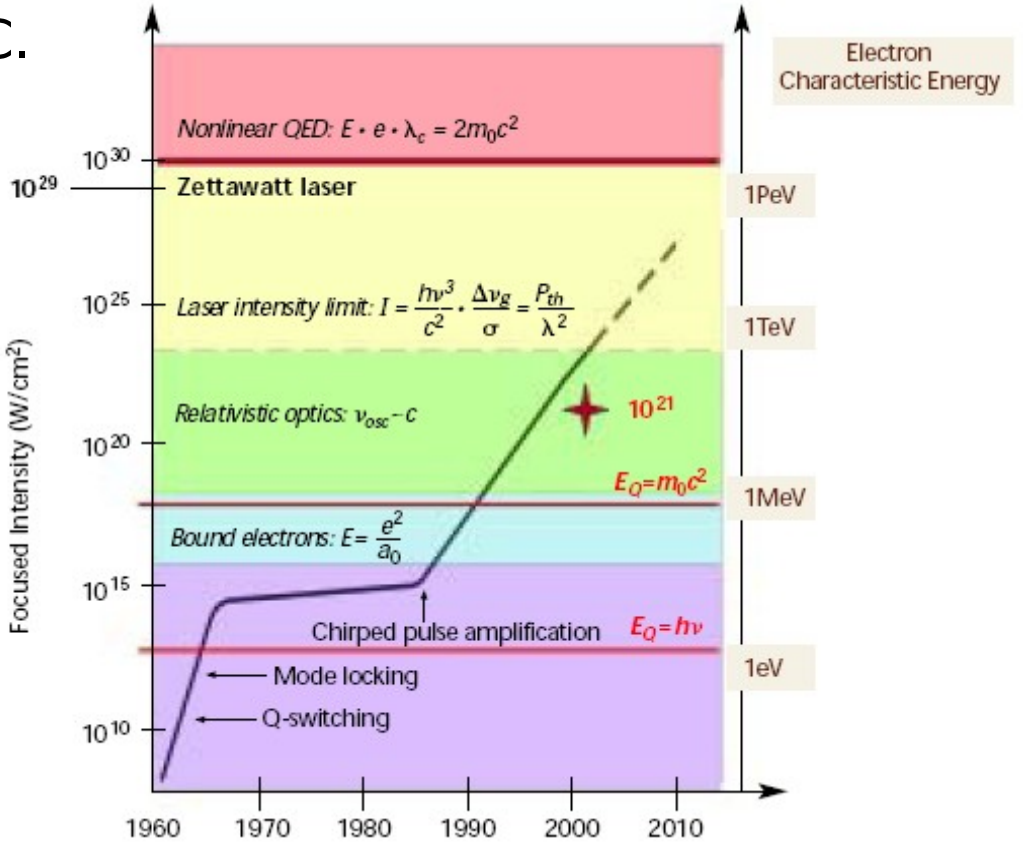

Laser-Matter Interaction Scenario @ $I=10^{20}$ W/cm^2

Electric field $E=\sqrt{4\pi\frac{I}{c}}=2.7\times10^{13}\ V/m=53\frac{e}{r_B^2}$ → **ultrafast ionization and plasma production**

Electron momentum $p_{osc}=\frac{eE}{\omega}=8.5\,m_e c\ @\ \lambda=1\,\mu m$ → **electrons are strongly relativistic**

Radiation pressure $P_{rad}=\frac{I}{c}=3.3\times10^{15}\ N/m^2$ → **radiation pressure dominates hydrodynamics**

Pulse duration may be
< 10 laser cycles
(e.g. 30 fs=3 x 10^{-14} s)
i.e the focused "laser beam" is a
light bullet

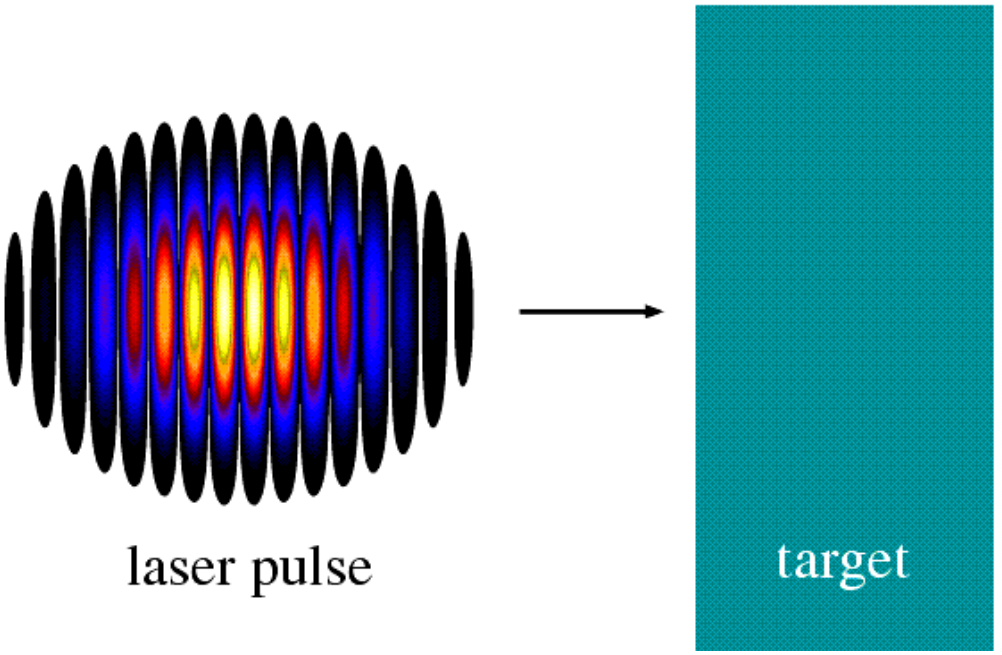

Related Definitions:
"*Extreme Light*", "*High Field Science*",
"*Relativistic Optics*",
"*High Energy Density Physics*" ...

G.Mourou, T.Tajima, S.V.Bulanov, Rev.Mod.Phys. **78** (2006) 309

The discovery of MeV proton emission in superintense interaction with *metallic* targets

Reported in 2000
by three experimental groups

[Clark et al, PRL **84** (2000) 670;
Maksimchuk et al, *ibid.*, 4108;
Snavely et al, PRL 85 (2000) 2945*]

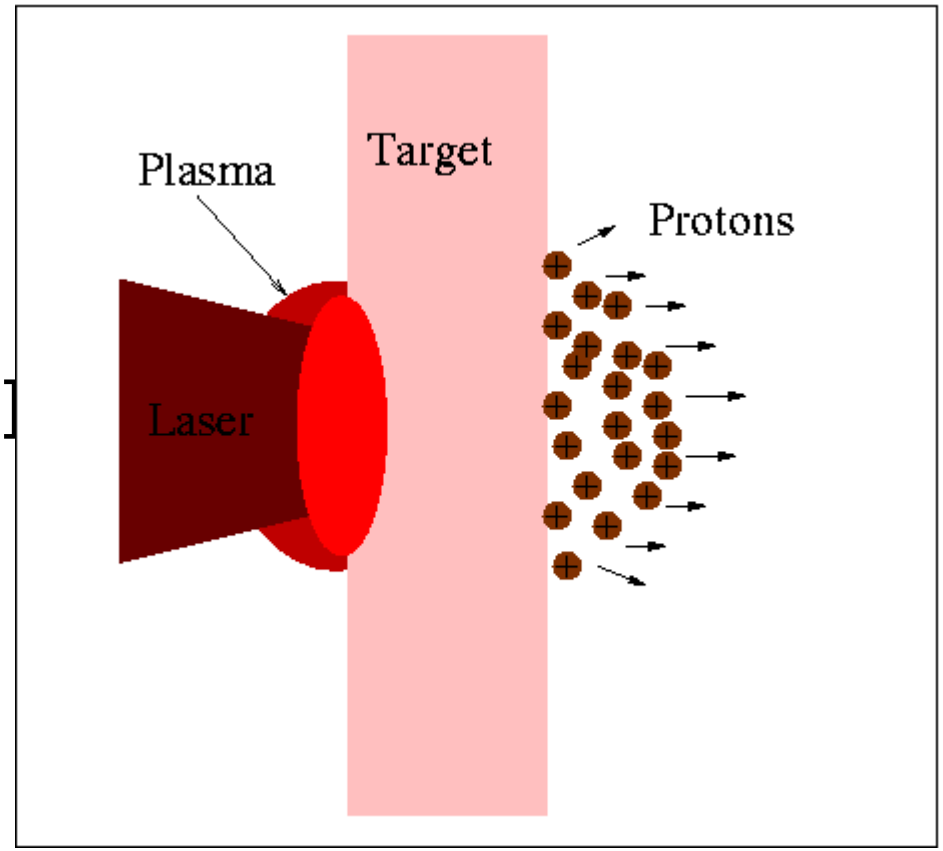

*** - 2 X 10^{13} protons with energy > 10 MeV, 58 MeV cut-off, good collimation (20°) conversion efficiency 12% of laser energy @ I=3 x 10^{20} W/cm^2**

The discovery of MeV proton emission in superintense interaction with *metallic* targets

Reported in 2000
by three experimental groups

[Clark et al, PRL **84** (2000) 670;
Maksimchuk et al, *ibid.*, 4108;
Snavely et al, PRL 85 (2000) 2945*]

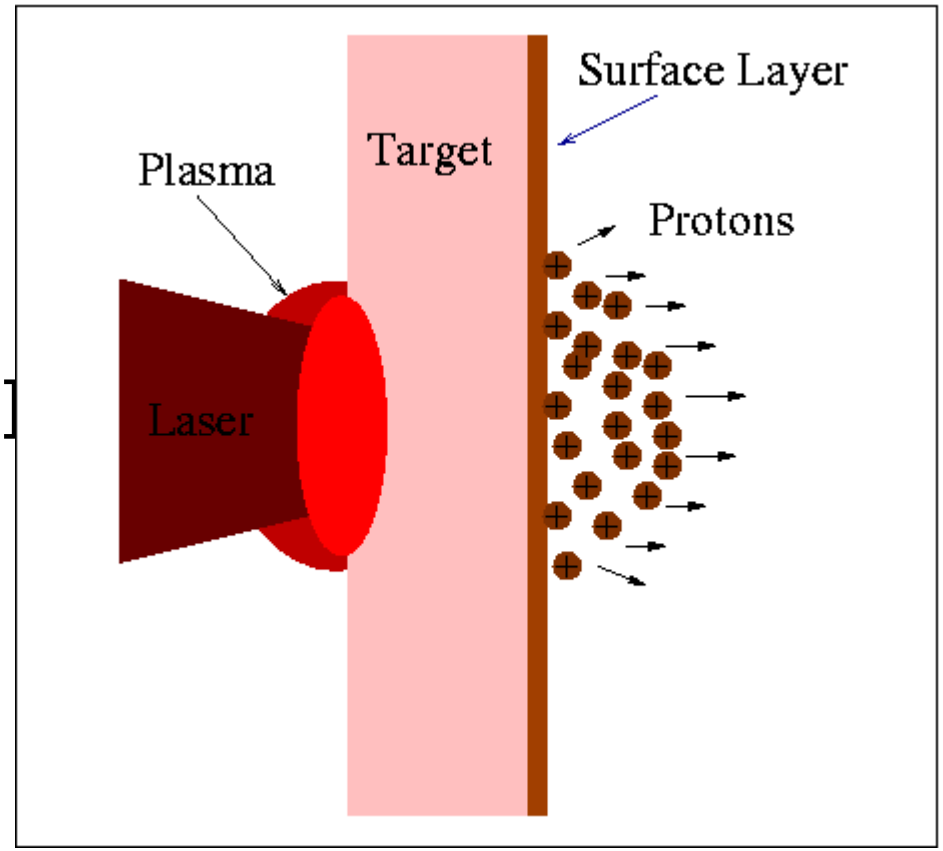

*** - 2 X 10^{13} protons with energy > 10 MeV, 58 MeV cut-off, good collimation (20°) conversion efficiency 12% of laser energy @ I=3 x 10^{20} W/cm²**

Question: origin of protons from metal?

Answer: hydrocarbon or water impurities on the target surface (e.g. from vacuum pump ...)

The discovery of MeV proton emission in superintense interaction with *metallic* targets

Reported in 2000
by three experimental groups

[Clark et al, PRL **84** (2000) 670;
Maksimchuk et al, *ibid.*, 4108;
Snavely et al, PRL 85 (2000) 2945*]

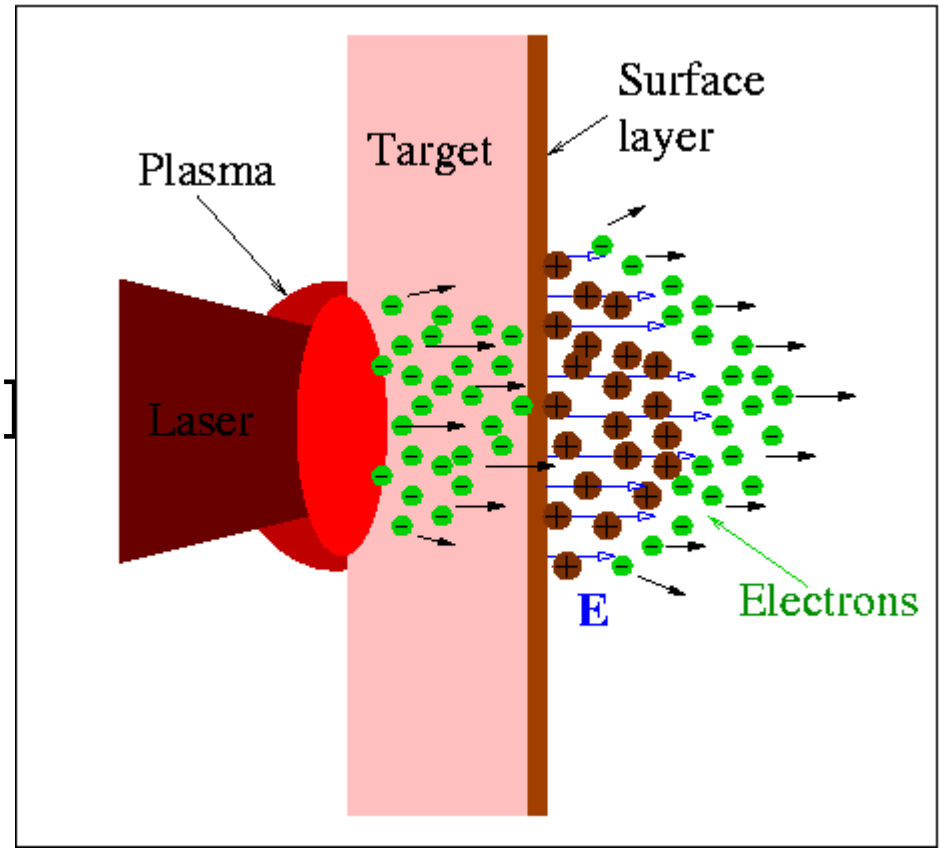

*** - 2 X 10^{13} protons with energy > 10 MeV, 58 MeV cut-off, good collimation (20°) conversion efficiency 12% of laser energy @ I=3 x 10^{20} W/cm^2**

Physical mechanism:
acceleration in the space-charge electric field generated by "fast" electrons escaping from the target (TNSA, Target Normal Sheath Acceleration)

MeV protons (ions) are appealing for applications requiring localized energy deposition in matter

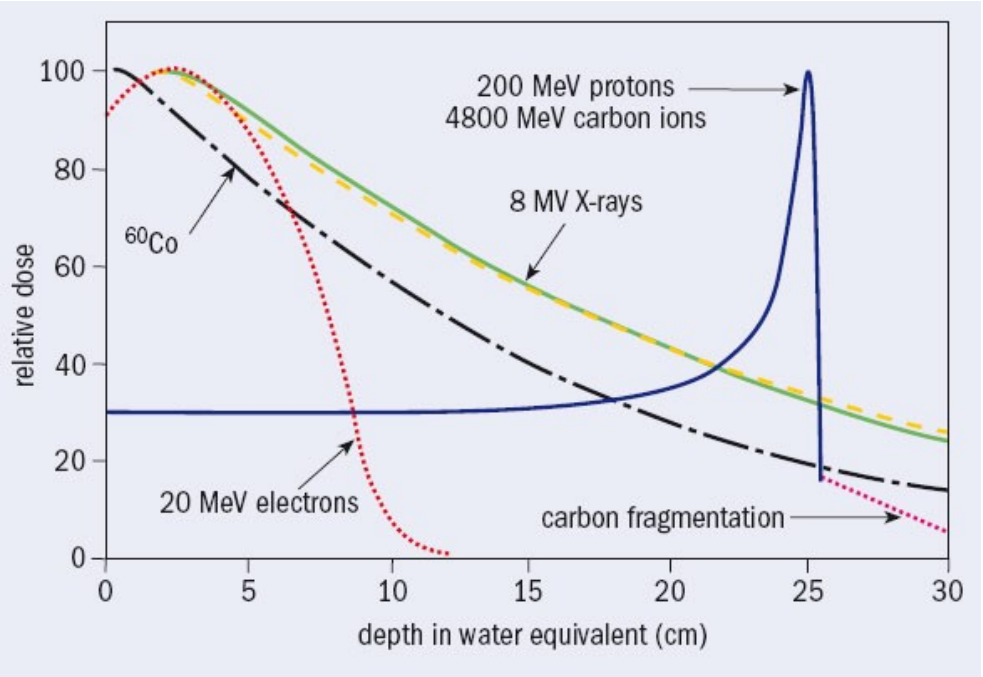

Sharp spatial maximum of deposited energy (Bragg peak)

Peak location depends on energy

[U. Amaldi & G. Kraft, Rep. Prog. Phys. **68** (2005) 1861]

MeV protons (ions) are appealing for applications requiring localized energy deposition in matter

Medical Applications

ONCOLOGICAL HADRONTHERAPY

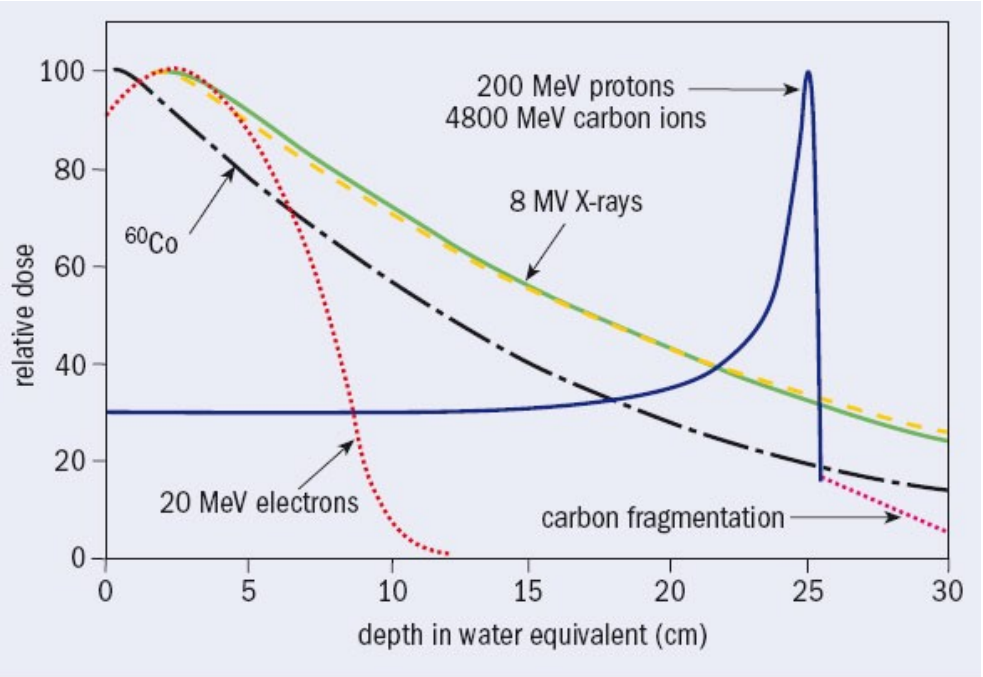

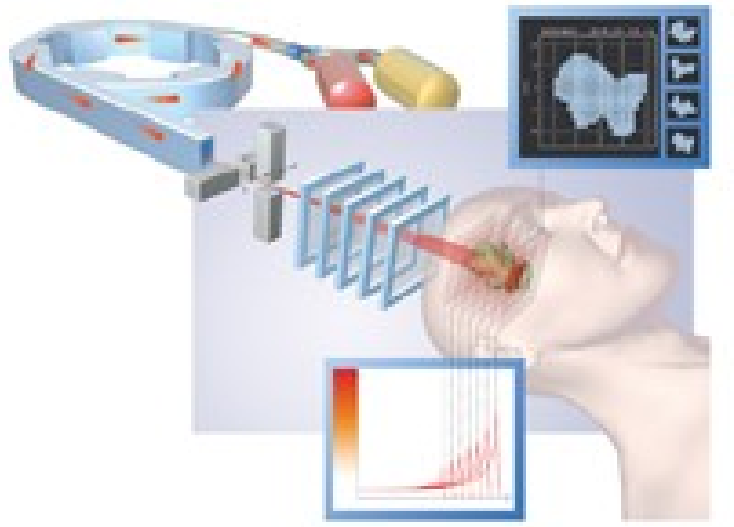

[U. Amaldi & G. Kraft, Rep. Prog. Phys. **68** (2005) 1861]

If feasible with table-top, high repetition lasers,
cost can be reduced with respect to an accelerator facility

Other foreseen application in medicine:
isotope production (e.g. for Proton Emission Tomography)

MeV protons (ions) are appealing for applications requiring localized energy deposition in matter

Inertial **C**onfinement **F**usion

FAST IGNITION

Protons can be used to create a "spark" in a pre-compressed ICF capsule achieving isochoric burn and high energy gain

[Roth et al, Phys. Rev. Lett. **86** (2001) 436;
Atzeni et al, Nuclear Fusion **42** (2002) L1]

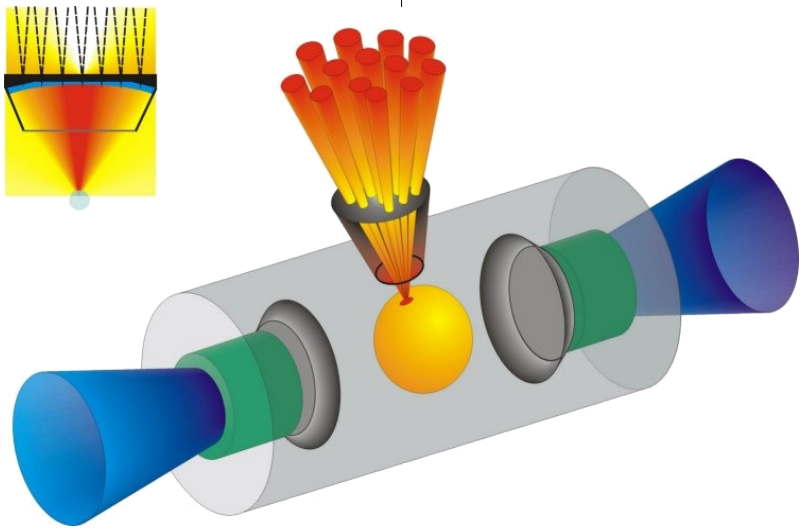

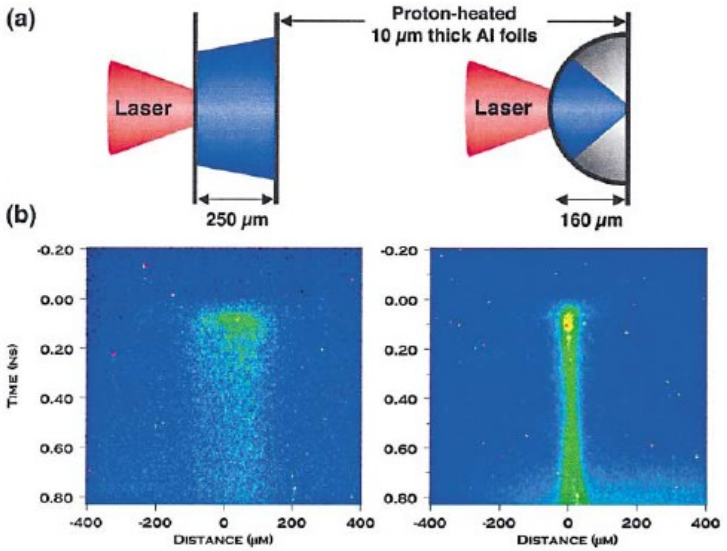

Geometrical focusing of laser-accelerated protons and localized isochoric heating has been demonstrated

[Patel et al, Phys. Rev. Lett. **91** (2003) 125004]

Experimental State of the Art (quick look)

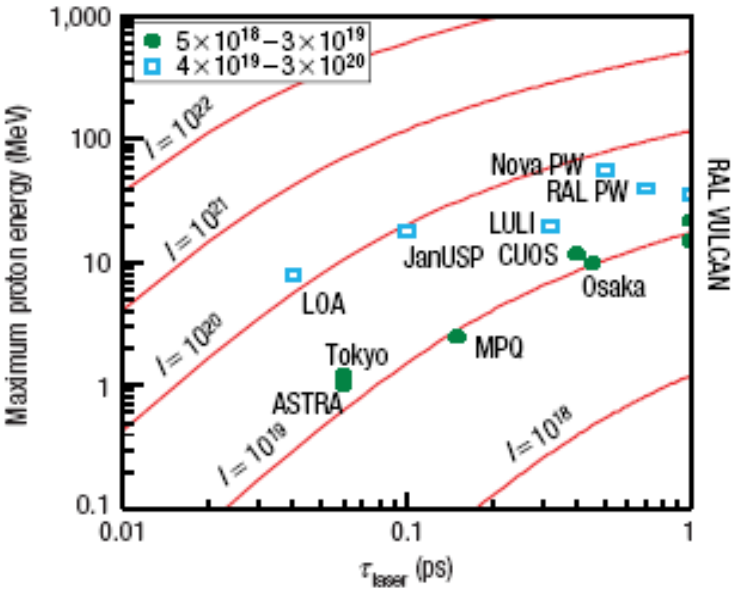

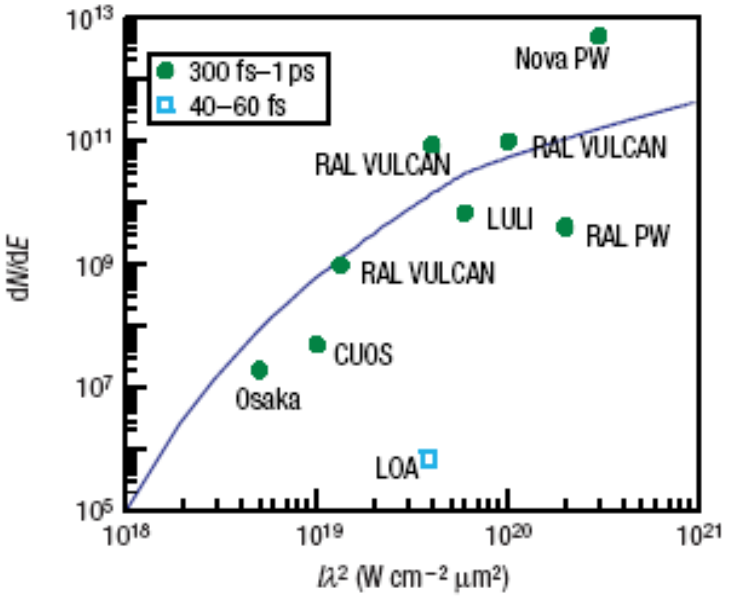

Scaling of ion energy and number is promising for medical and fusion applications

From: M.Borghesi et al, Fusion Science & Technology **49** (2006) 412;
J. Fuchs et al, Nature Physics **2** (2005) 48 .

Most recent results:

- narrow energy spectrum of protons from engineered double-layer target
[H. Schwoerer et al, Nature **439** (2006) 445]

- MeV carbon ions from pre-heated (“decontaminated”) target
[B. Hegelich et al, Nature **439** (2006) 441]

- Ultrafast “laser-plasma microlens” for ion beam focusing and energy selection
[Toncian et al, Science **312** (2006) 410]

The development of the Proton Imaging technique to detect highly transient ElectroMagnetic fields

Properties of the proton source

Imaging properties of the emitted protons are those of a **point-like virtual source**

Proton beam is **quasi-laminar** (**ultra-low emittance**)

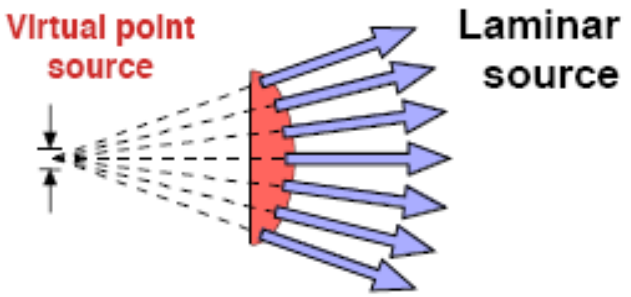

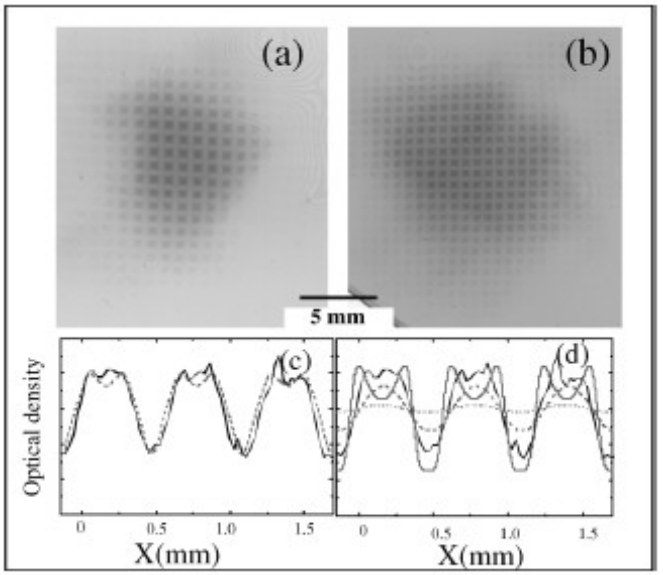

Shadow of micrometric grid mesh with 15 MeV protons provides magnification test and estimate of source dimensions $a < 10$ μm
[Borghesi et al, PRL **92** (2004) 055003]

$a = 1.4$ μm reported at lower energy
[Cobble et al, J.Appl.Phys. **92** (2002) 1775]

Imaging of thin objects possible due to multiple small-angle scattering of protons
[West & Sherwood, Nature **239** (1972) 157]

Transverse emittance measurement for >10 MeV protons
[Cowan et al, PRL **92** (2004) 204801]

$\varepsilon < 4 \times 10^{-3}$ mm mrad

Energy resolving allows temporal resolution

Use of RadioChromic Film (RCF) stack as a detector allows single-shot, spatial and **energy** resolution of the proton beam

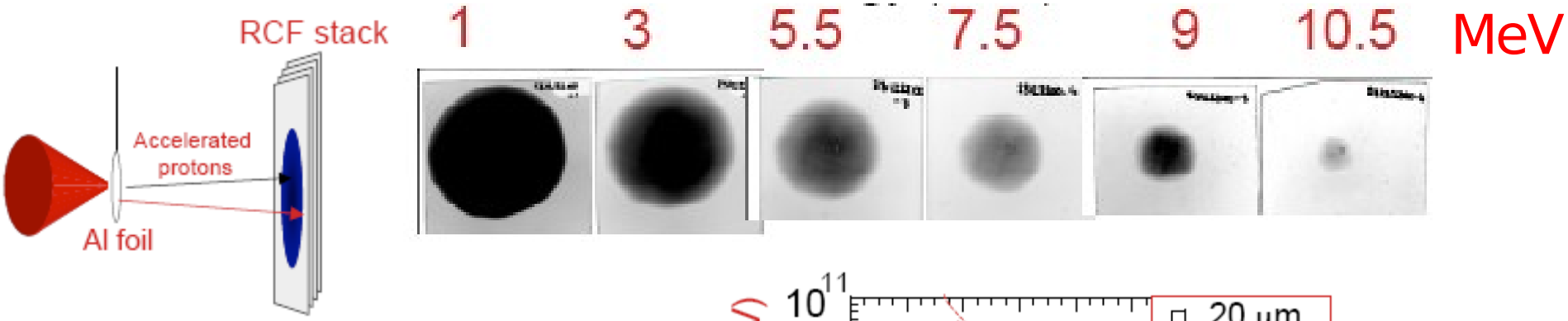

Typical data example

(taken at the LULI 100 TW facility, École Polytechnique, Palaiseau, France)

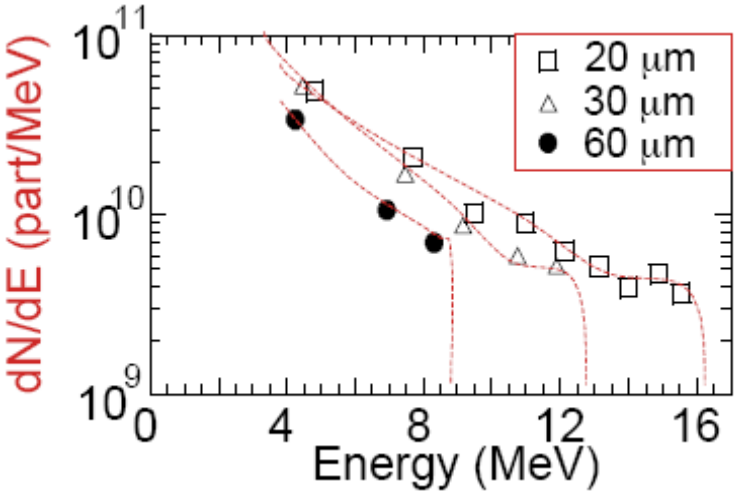

RCF energy selection capability is another consequence of Bragg peak deposition

Energy resolving allows temporal resolution

Use of RadioChromic Film (RCF) stack as a detector allows single-shot, spatial and **energy** resolution of the proton beam

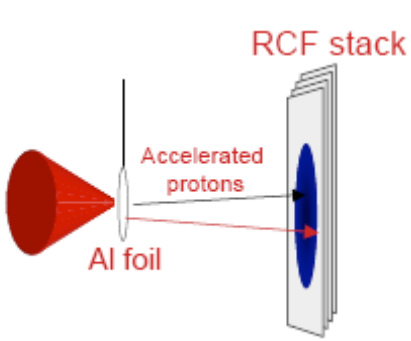

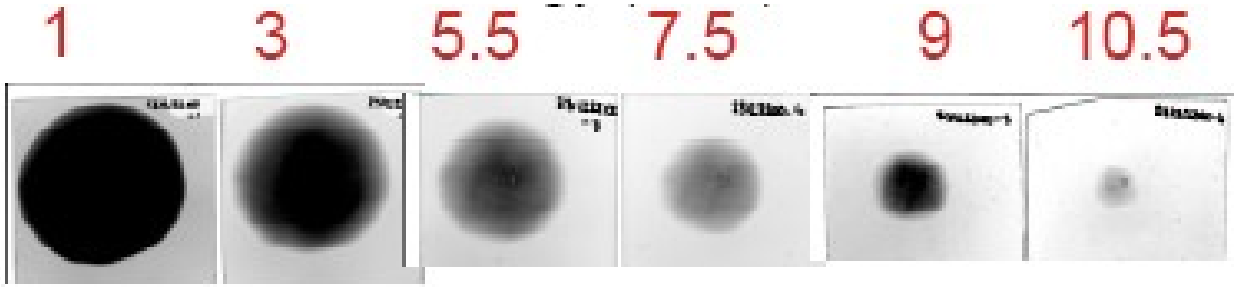

72 42 31 26 24 22 ps

In a time-of-flight arrangement protons of different energies cross the object at different times: imaging of transient objects possible

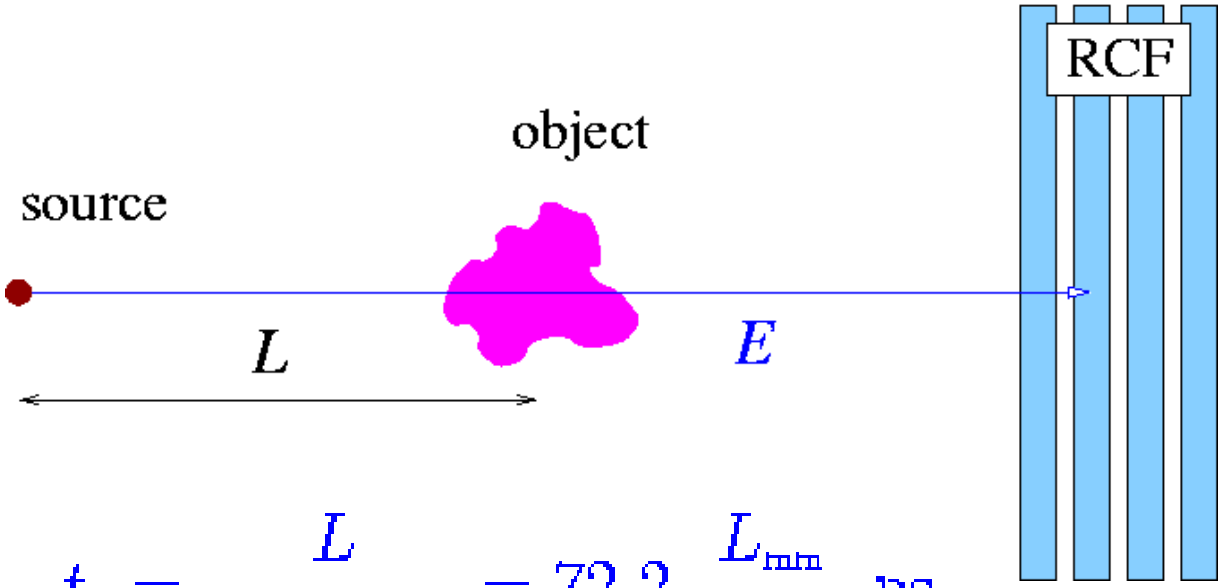

RCF energy bandwidth allows picosecond resolution

$$t_p = \frac{L}{\sqrt{2E/m_p}} = 72.2\frac{L_{\mathrm{mm}}}{\sqrt{E_{\mathrm{MeV}}}}\mathrm{ps}$$

Using protons to detect EM fields

A proton crossing an EM field distribution acquires a transverse velocity $\delta\mathbf{v}$

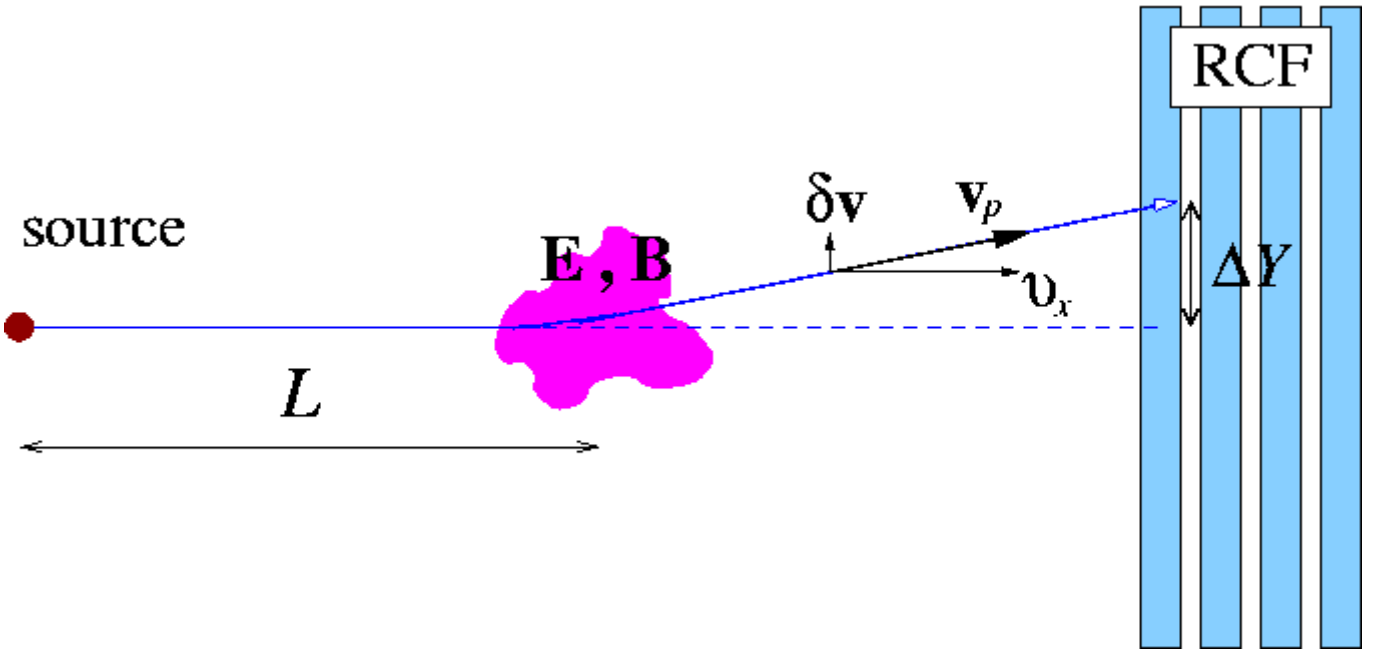

$$\delta\mathbf{v} = \frac{e}{m_p}\int (\mathbf{E} + \mathbf{v}_p \times \mathbf{B})\, dt$$

For *weak* deflections (1st order Born approximation)

$$v_x = \frac{dx}{dt} \simeq v_p \quad \rightarrow \quad \delta Y = |\delta\mathbf{v}_\perp|\Delta t \simeq \frac{eL}{2\mathcal{E}_p}\int (\mathbf{E} + \mathbf{v}_p \times \mathbf{B})_\perp\, dx$$

Concept: estimate $\mathbf{E}$ (and/or $\mathbf{B}$) from the measurement of ΔY

Using protons to detect EM fields

A proton crossing an EM field distribution acquires a transverse velocity $\delta\mathbf{v}$

$$\delta\mathbf{v} = \frac{e}{m_p}\int (\mathbf{E} + \mathbf{v}_p \times \mathbf{B})\, dt$$

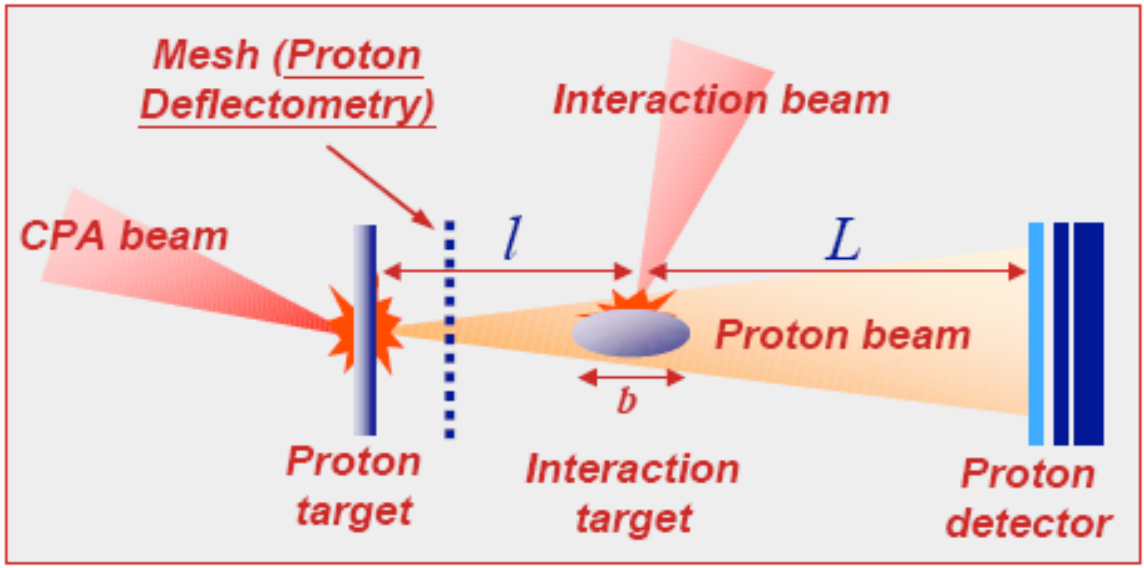

The technique is particularly attractive for laser-plasma interaction experiments because of:

- absence of other field-sensitive diagnostics
- high spatio-temporal resolution
- single-shot capability
- easy sinchronization of probe with an interaction pulse

Proton “Deflectometry”

The proton deflection ΔY can be measured directly by the deformation of the imprint of a stopping mesh

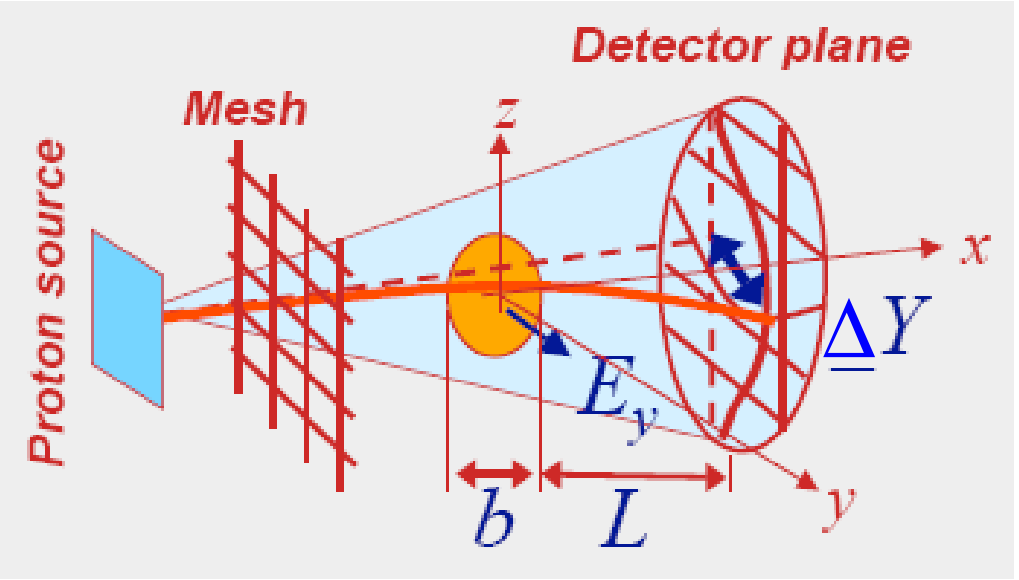

Assuming that only E contributes we estimate the average field as

$$\langle \mathbf{E} \rangle \simeq \frac{1}{b} \int_{-b/2}^{+b/2} \mathbf{E}_{\perp} dx \simeq \frac{2\mathcal{E}_p}{eLb} \Delta Y$$

Proton “Imaging”

When fields gradients are present deflections produce a modulation δn in the proton density n_p on the detector plane:

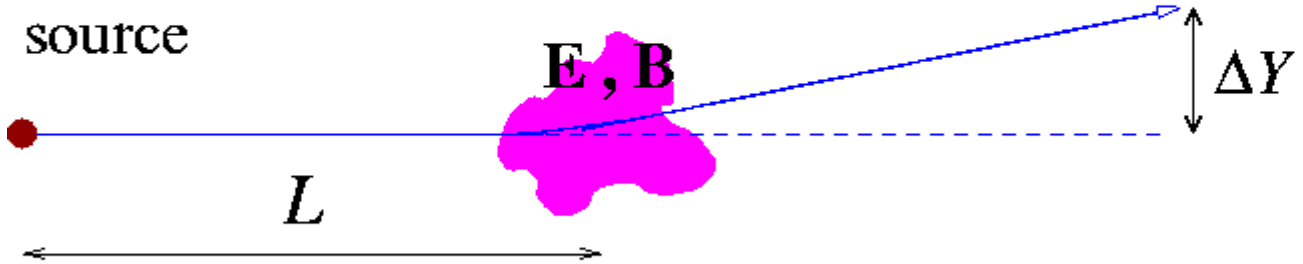

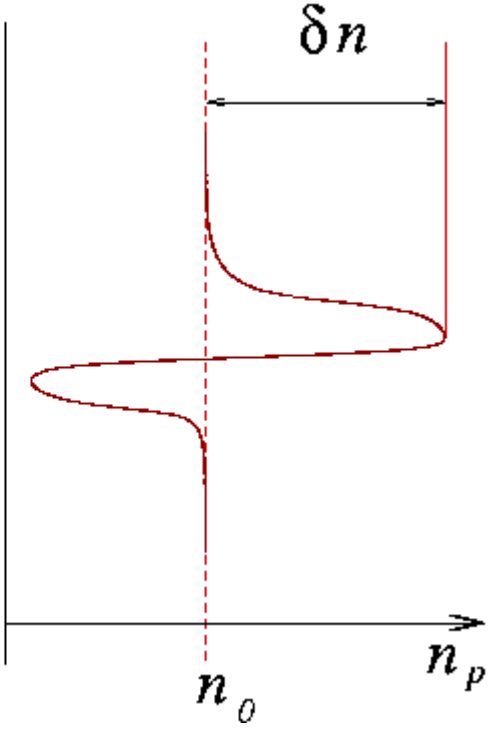

The observed modulation δn is proportional to the line integral of “source” terms

(M : geometrical magnification)

$$\frac{\delta n}{n_0} \simeq -\frac{1}{M}\nabla_\perp \cdot \Delta \mathbf{Y} \simeq -\frac{2\pi e L b}{\mathcal{E}_p M}\int_{-b/2}^{+b/2}\left(\rho - \frac{1}{c^2}\mathbf{v}_p \cdot \mathbf{J}\right) dx$$

Modeling of “proton diagnostic experiments”

Interpretation of proton diagnostic data usually occurs through three steps:

1. Find a model (analytical and/or numerical) for the electric field $\mathbf{E}(x,t)$ [and/or the magnetic field $\mathbf{B}(x,t)$]

   - frequent need to bridge the gap between temporal scales or dimensionality of laser-plasma “ab initio” simulations (particle-in-cell method) and those of the experiment:

   fs ➞ ps , 2D ➞ 3D

2. Simulate the proton diagnostic via particle tracing simulations with $\mathbf{E}(x,t)$ as an input

3. Compare simulated proton images with experimental ones

Investigations of laser-plasma phenomena based of field detection by Proton Imaging/Deflectometry

- sheath acceleration
- self-channeling
- coherent structure formation

Detection of Proton-Accelerating Sheath Fields

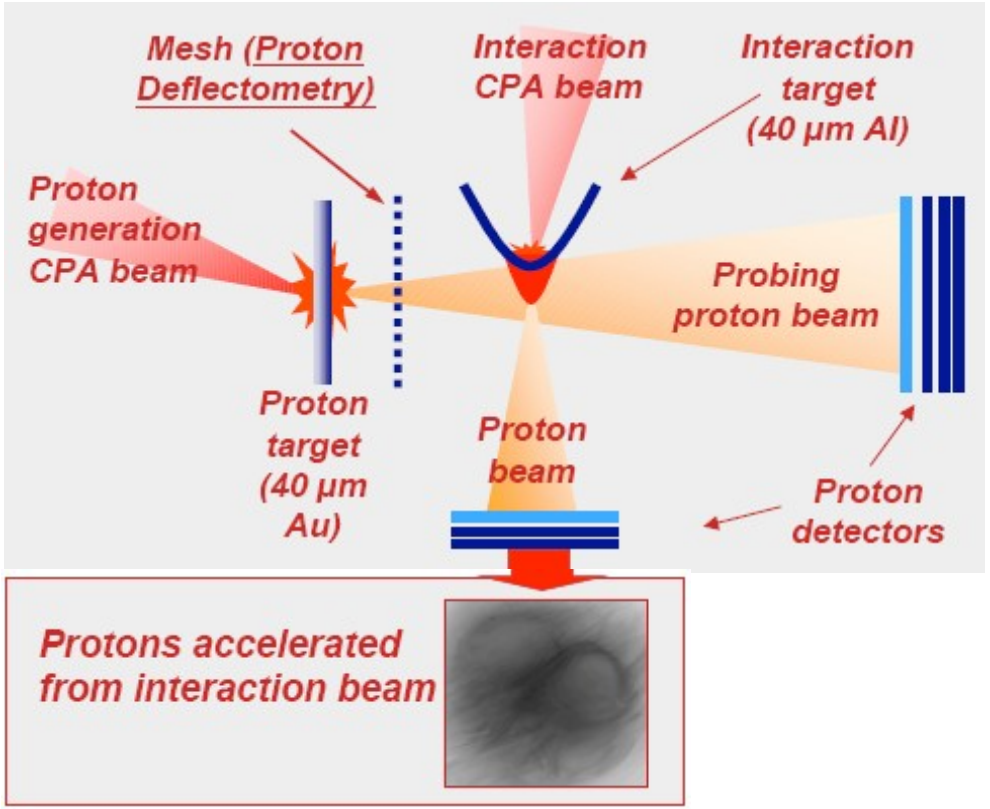

Goal: study of TNSA mechanism for ion acceleration
by the direct detection of related space-charge electric field

Technique: use a second proton beam as a transverse probe

Detection of Proton-Accelerating Sheath Fields

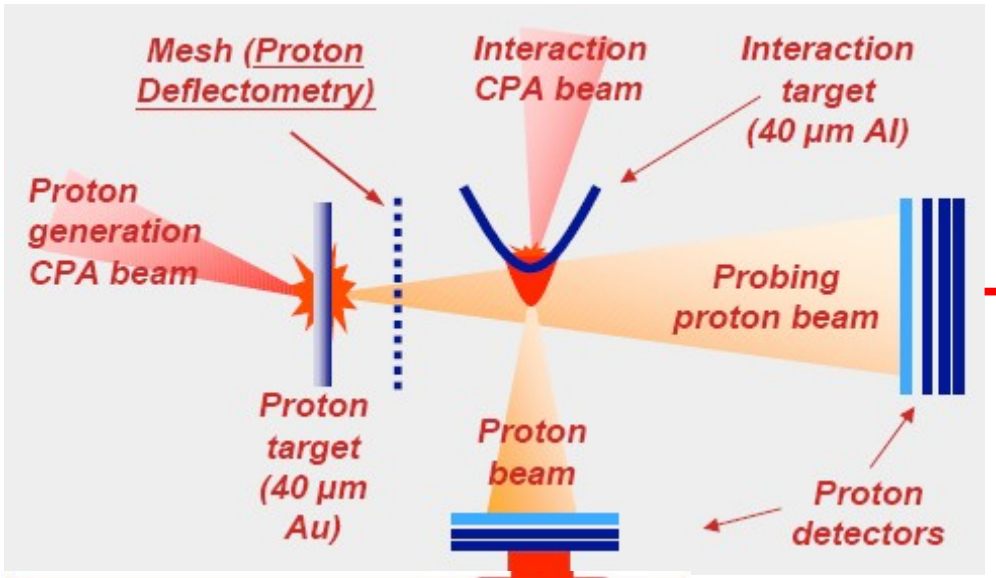

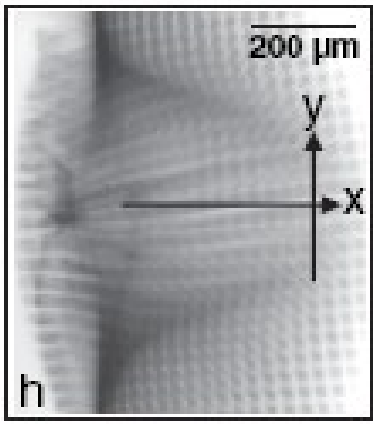

11 ps

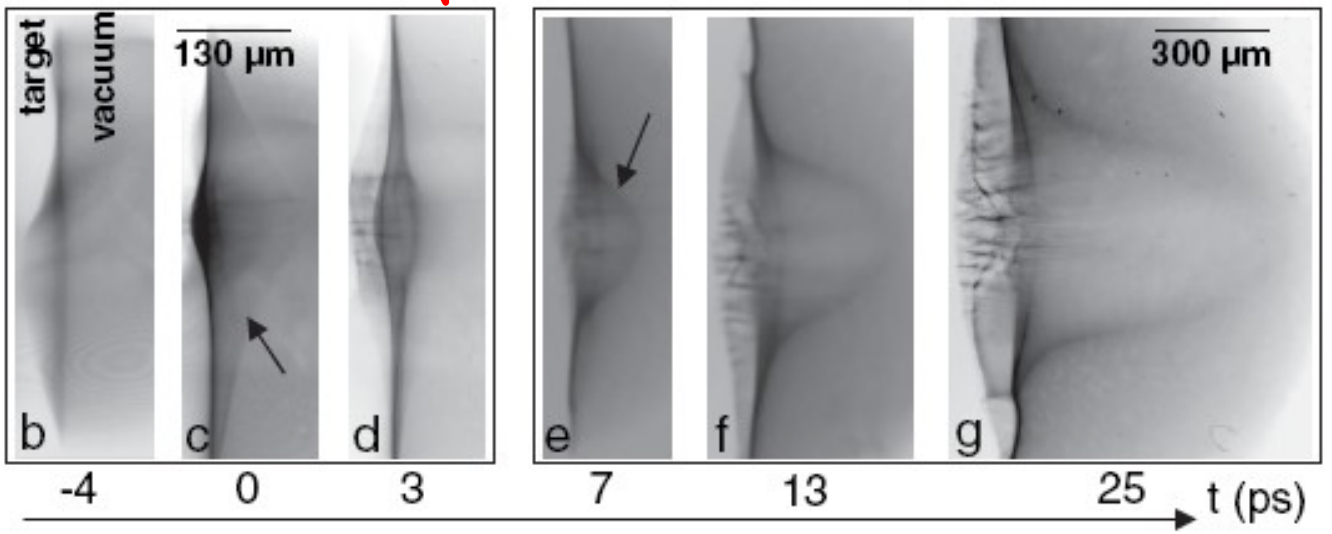

Expanding, bell-shaped front observed in proton images and deflectograms

L. Romagnani, J. Fuchs, M. Borghesi, P. Antici, P. Audebert, F. Ceccherini, T. Cowan, T. Grismayer, S. Kar, A. Macchi, P. Mora, G. Pretzler, A. Schiavi, T. Toncian, O. Willi, Phys. Rev. Lett. **95** (2005) 195001

Modeling of sheath acceleration: the problem of plasma expansion in vacuum

Analytical approach:

- electrostatic approximation
- fluid ions
- electrons in Boltzmann equilibrium

$$n_e = n_0 \exp\left(\frac{e\Phi}{k_B T_e}\right), \qquad \nabla^2\Phi = Zen_i - en_e$$

$$M_i \frac{d\mathbf{v}_i}{dt} = Ze\mathbf{E} = -Ze\boldsymbol{\nabla}\Phi, \quad \partial_t n_i = \boldsymbol{\nabla}\cdot(n_i\mathbf{v}_i)$$

Numerical PIC approach:

- electrostatic approximation
- kinetic ions and electrons
- “fast” electron temperature and density as input parameters

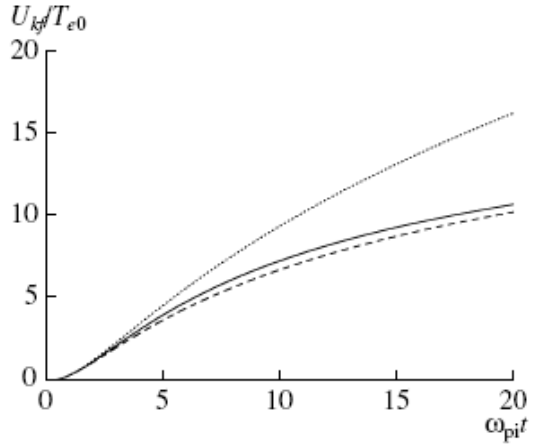

Fig. 3. The kinetic energy acquired by the fastest ion during the expansion of a slab of total thickness $2a = 40$ as predicted by the numerical simulations (solid line), by the analytical model (dashed line), and by the semi-infinite model [11] (dotted line).

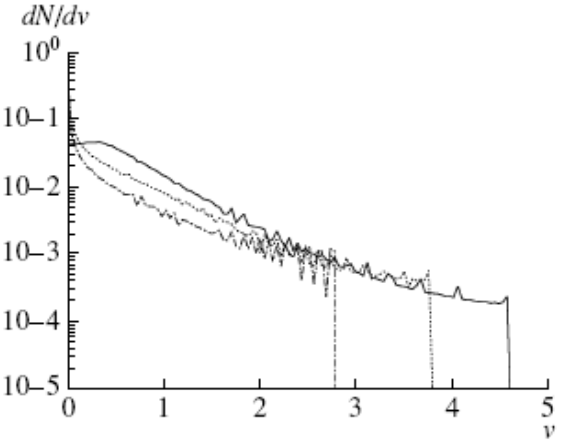

Fig. 4. Ion velocity spectrum at $\tau = 5$ (dashed line), $\tau = 10$ (dotted line), and $\tau = 20$ (solid line). The initial slab total size is $2a = 40$ and v is normalized to the initial sound speed.

S.Betti, F.Ceccherini, F.Cornolti, F.Pegoraro, Plasma Phys. Control. Fusion **47** (2005) 521
F.Ceccherini, S.Betti, F.Cornolti, F.Pegoraro, Laser Physics **16** (2006) 1

Comparison with experiment supports TNSA modeling

Experimental results have been compared with PIC simulations using the plasma expansion model.

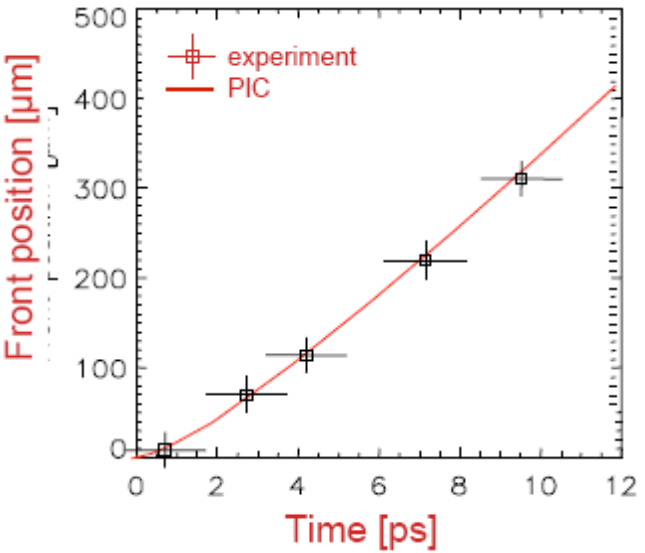

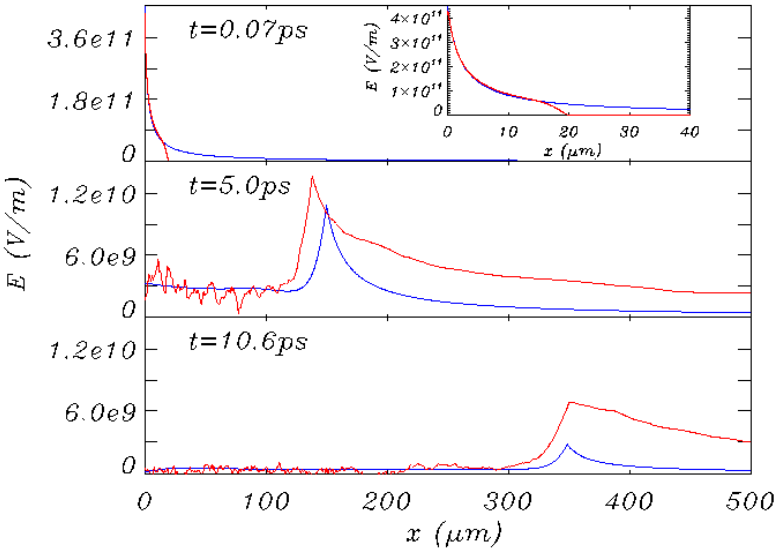

Particle tracing simulations of proton deflection in the PIC fields well reproduce experimental images and deflectrograms

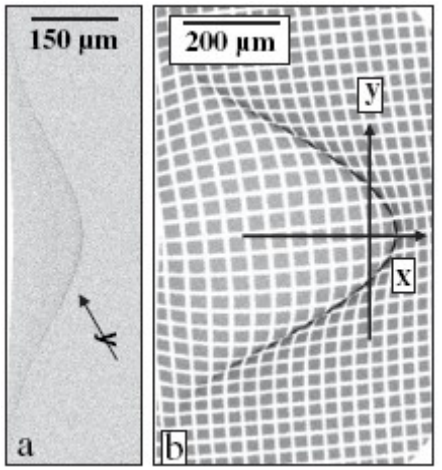

Comparison of fluid and kinetic (PIC) results show the importance of kinetic and non-thermal effects in the plasma expansion

L. Romagnani, J. Fuchs, M. Borghesi, P. Antici, P. Audebert, F. Ceccherini, T. Cowan, T. Grismayer, S. Kar, A. Macchi, P. Mora, G. Pretzler, A. Schiavi, T. Toncian, O. Willi, Phys. Rev. Lett. **95** (2005) 195001

Study of charge-displacement self-channeling

Theory predicts that a superintense laser pulse propagating in a low-density plasma undergoes self-focusing and channeling due to both relativistic effects and radial plasma expulsion by the radial ponderomotive force (i.e. radiation pressure)

For a transient stage the channel is charged since electrons are expelled first. No “direct” diagnostic of this regime was available before!

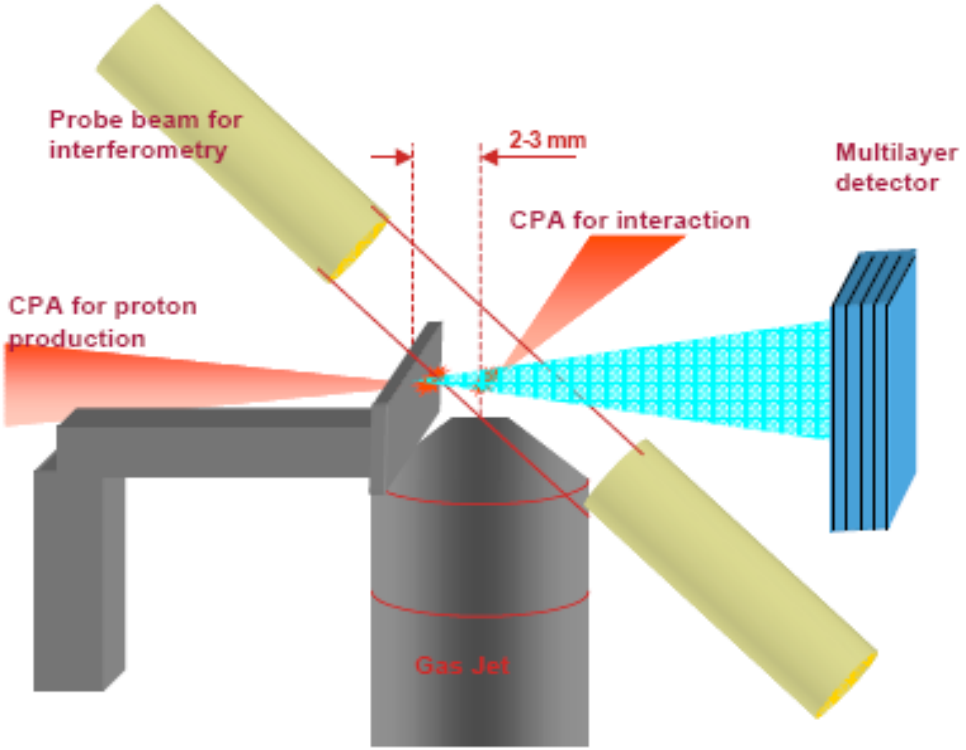

Set-up for proton probing and preformed plasma density characterization by interferometry

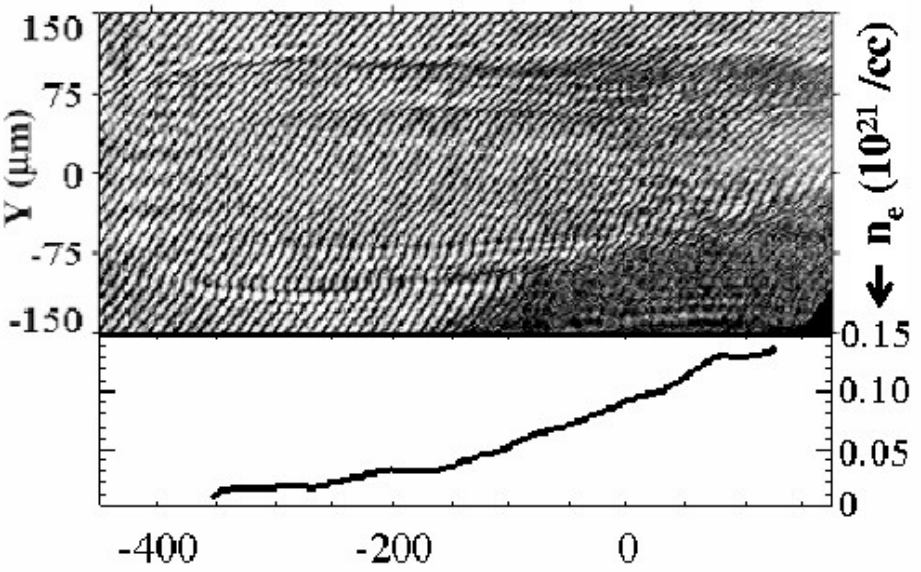

Proton images of charged channel evolution

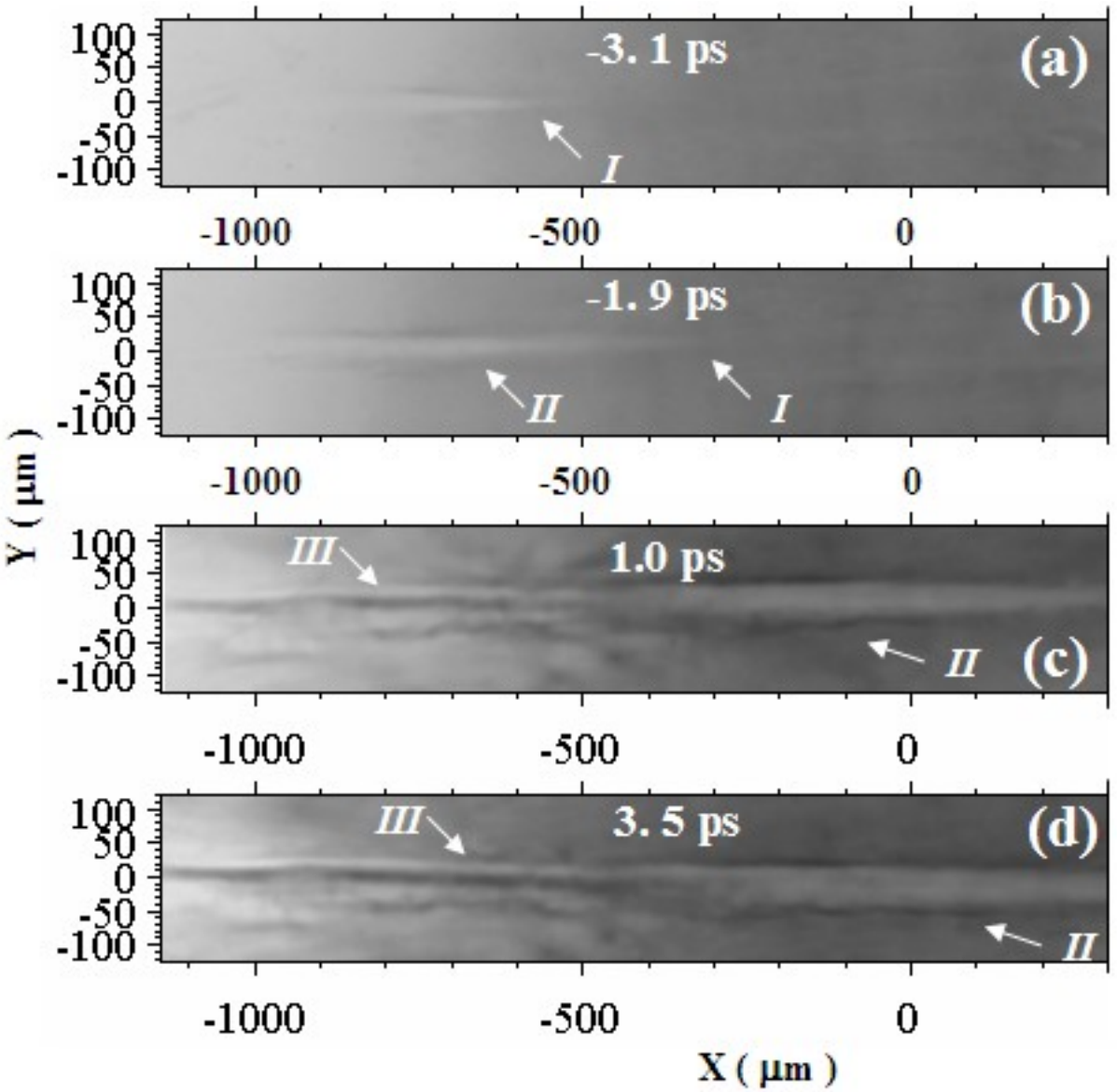

Early times (during the laser pulse) propagating "white" channel front indicates electron expulsion from the axis

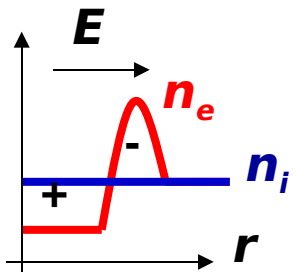

Late times (after the laser pulse) "black" line on axis indicates field inversion at some location

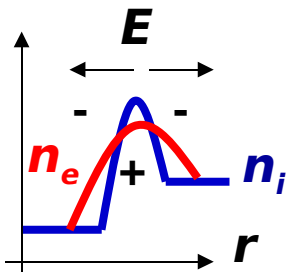

S.Kar, M.Borghesi, C.A.Cecchetti, L.Romagnani, F.Ceccherini, T.V.Lyseikina, A. Macchi, R.Jung, J.Osterholz, O.Willi, M.Galimberti, L.A.Gizzi, A.Schiavi, R.Heathcote, submitted to Nature Physics (arXiv:physics/0701332)

Channel front propagation speed

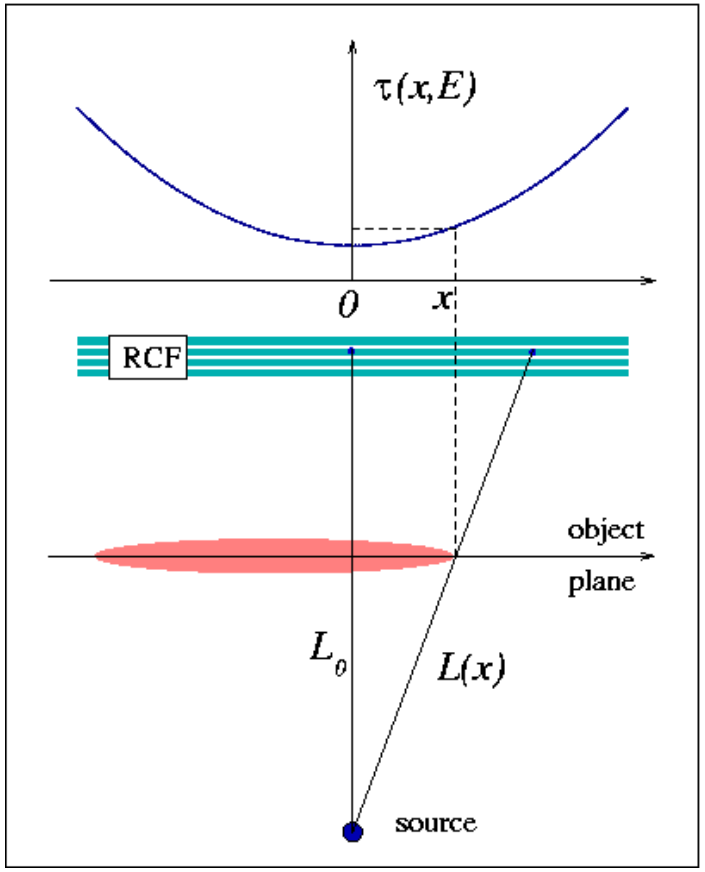

Due to the divergence of the proton beam the "probing time" depends on angle (i.e. on the position on the object plane)

$$\tau(x,E) = t_0(E) + \frac{L_0}{\sqrt{2E/m_p}}\left(\sqrt{1+x^2/L_0^2}-1\right)$$

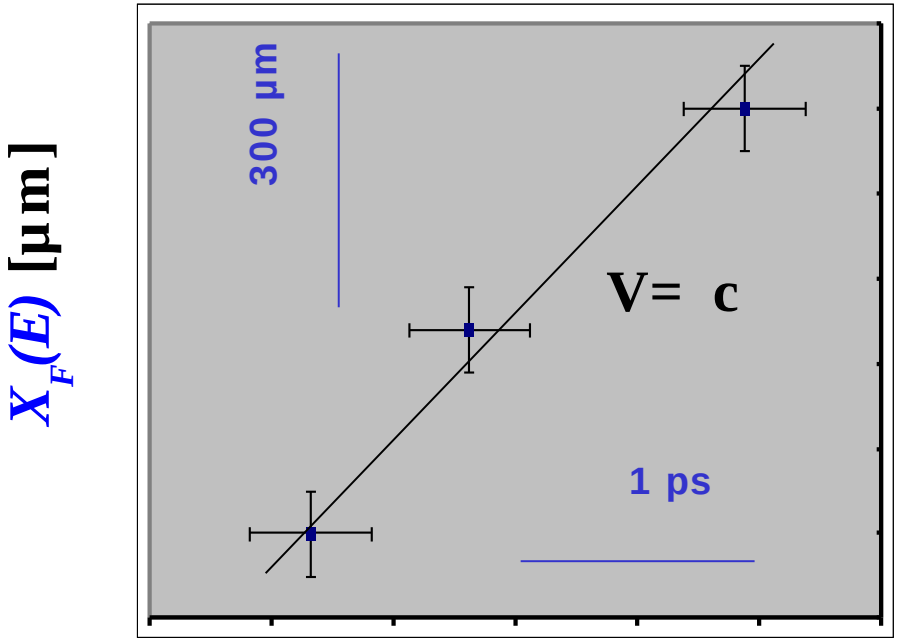

Plotting the channel front displacement $X_F(E)$ *vs.* the probing time $\tau(X_F,E)$ we obtain the front propagation speed $V \sim c$

2D PIC simulations show “radial” field dynamics

Laser

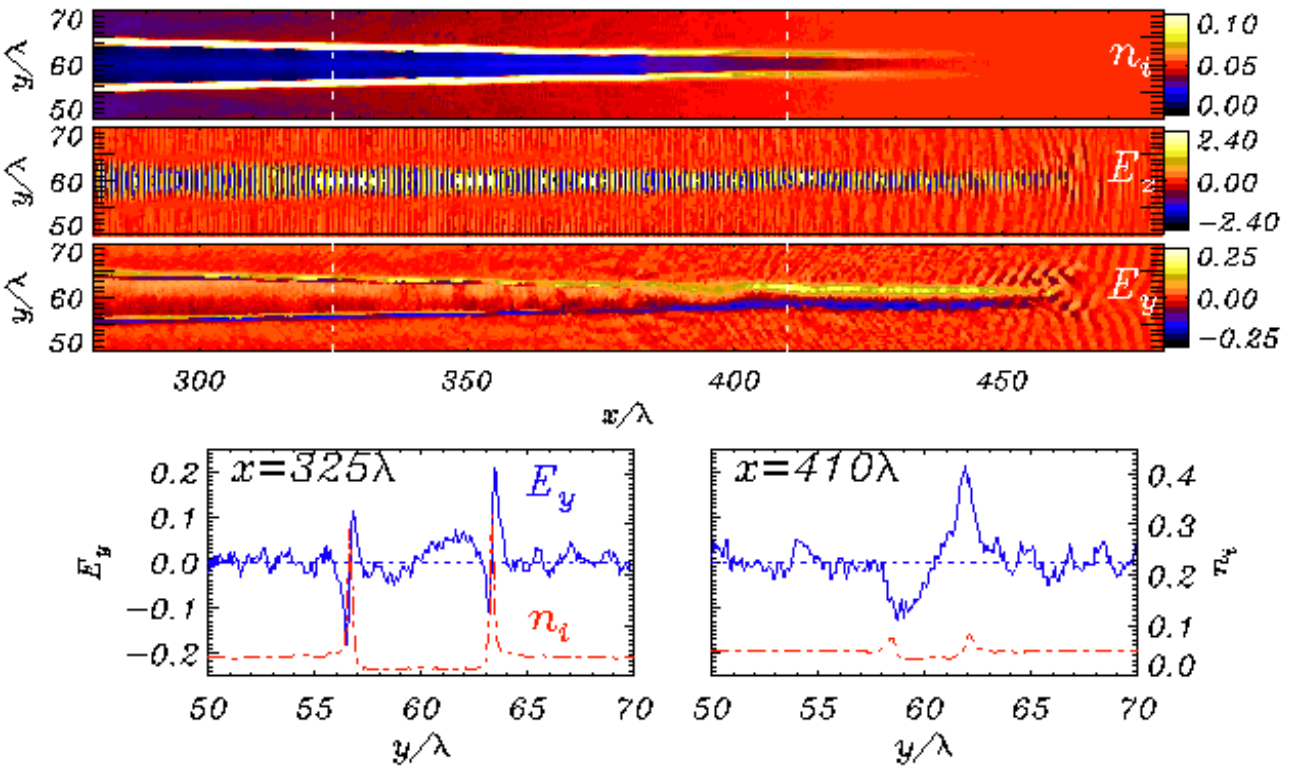

Two ambipolar fronts of E_y appear in the trailing edge of the channel; “negative” part can produce “black line” in proton images

Outward-directed radial field E_y due to electron expulsion from axis

EM component E_z reveals self-focusing

S.Kar, M.Borghesi, C.A.Cecchetti, L.Romagnani, F.Ceccherini, T.V.Lyseikina, A. Macchi, R.Jung, J.Osterholz, O.Willi, M.Galimberti, L.A.Gizzi, A.Schiavi, R.Heathcote, submitted to Nature Physics (arXiv:physics/0701332)

Ponderomotive model of self-channeling

Assumptions:
- cylindrical symmetry
- non-evolving laser pulse
- electrostatic approximation

Solution based on kinetic PIC model

$$
\begin{aligned}
m_e dv_e/dt &= -eE_r - m_e c^2 \partial_r \sqrt{1+a^2} \\
a = a(x,r,t) &= a_0 e^{-r^2/r_0^2 - (x-ct)^2/c^2\tau^2} \\
m_i dv_i/dt &= ZeE_r \\
\frac{1}{r}\partial_r (r \cdot E_r) &= 4\pi e(Zn_i - n_e)
\end{aligned}
$$

Particle tracing simulations using $\mathbf{E}$ from PIC model well reproduce experimental features

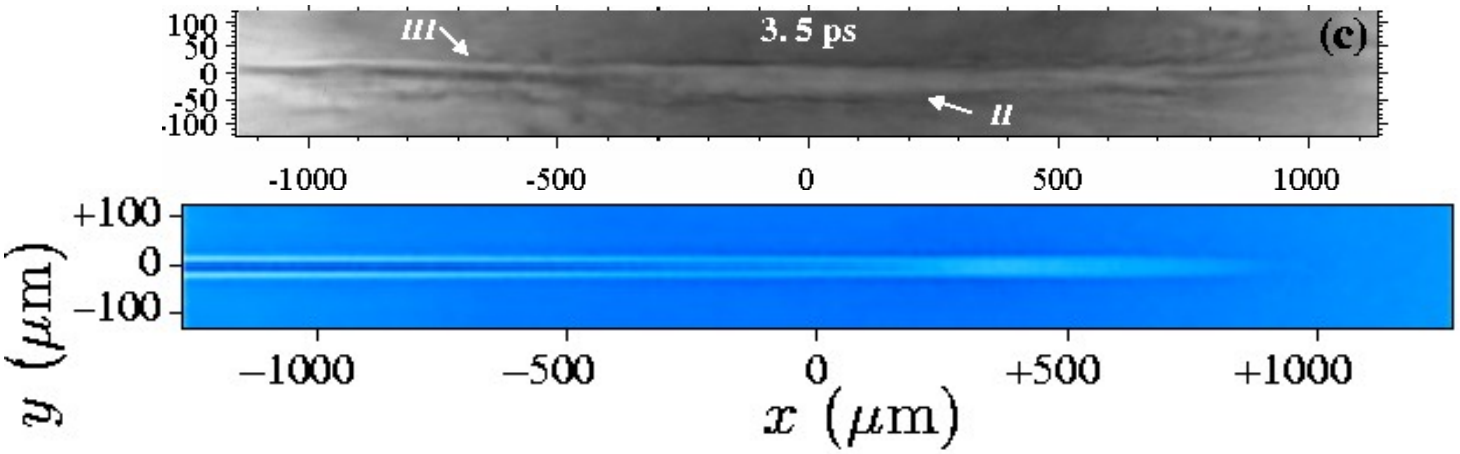

S.Kar, M.Borghesi, C.A.Cecchetti, L.Romagnani, F.Ceccherini, T.V.Lyseikina, A. Macchi, R.Jung, J.Osterholz, O.Willi, M.Galimberti, L.A.Gizzi, A.Schiavi, R.Heathcote, submitted to Nature Physics (arXiv:physics/0701332)

Ponderomotive model of self-channeling

Assumptions:
- cylindrical symmetry
- non-evolving laser pulse
- electrostatic approximation

Solution based on kinetic PIC model

$$m_e dv_e/dt = -eE_r - m_e c^2 \partial_r \sqrt{1+a^2}$$
$$a = a(x,r,t) = a_0 e^{-r^2/r_0^2 - (x-ct)^2/c^2\tau^2}$$
$$m_i dv_i/dt = ZeE_r$$
$$\frac{1}{r}\partial_r (r \cdot E_r) = 4\pi e(Zn_i - n_e)$$

The late ambipolar field appears after the vanishing of the early field ("echo" effect) due to hydrodynamical breaking in the ion density profile causing strong electron heating

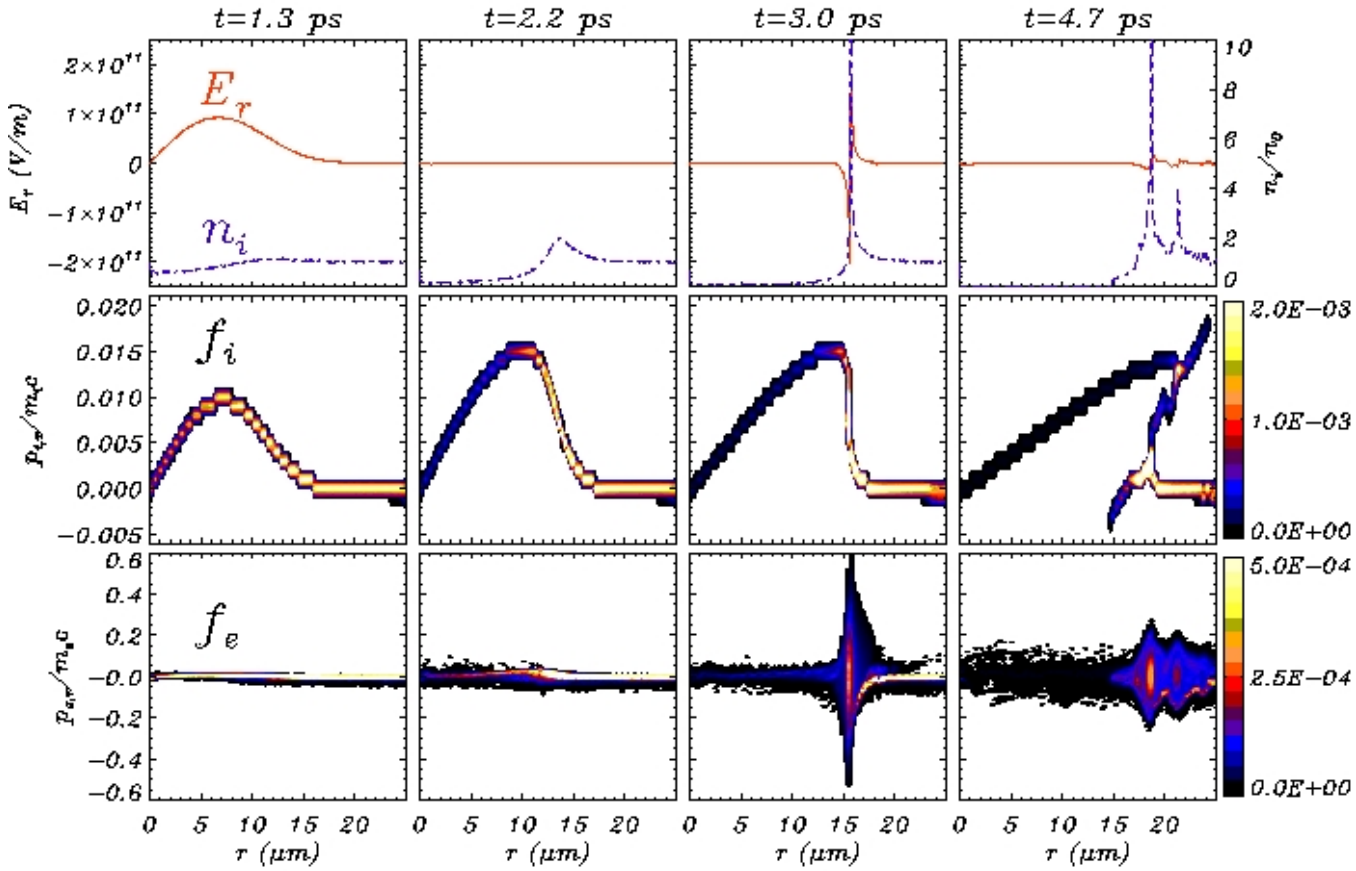

A. Macchi, F.Ceccherini, F. Cornolti, S.Kar, M.Borghesi, arXiv:physics/0701139

Study of “coherent”, long-lived field structures

Theory and numerical simulations show that a variety of slowly varying structures (**solitons**, **vortices**, **cavitons** ...) is generated during laser-plasma interactions.

Bubble-like structures interpreted as remnants of **relativistic solitons** (“post-solitons”)

[Borghesi et al., Phys. Rev. Lett. **88** (2002) 135002]

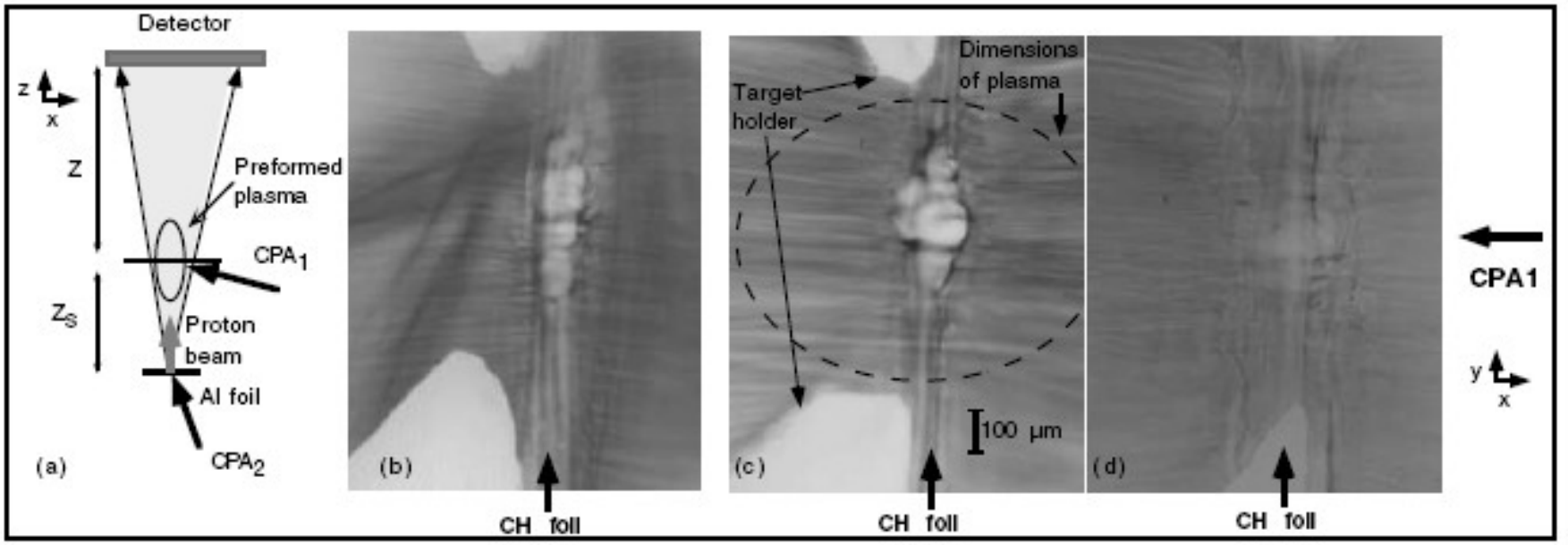

FIG. 1. (a) Experimental arrangement. (b), (c), (d) Proton images of the preformed plasma taken with 6–7 MeV protons, respectively: (b) 25 ps; (c) 45 ps; (d) 95 ps after the CPA_1 interaction. The scale refers to dimensions in the object plane. The dashed line indicates the dimensions of the preformed plasma defined by $n \approx 0.01 n_{cr}$ (at $\lambda = 1\ \mu$m).

Study of “coherent”, long-lived field structures

Theory and numerical simulations show that a variety of slowly varying structures (**solitons**, **vortices**, **cavitons** ...) is generated during laser-plasma interactions.

Ion modulations resulting from onset and evolution of **Buneman instability** in the late evolution of a plasma wake

[Borghesi et al., Phys. Rev. Lett. **94** (2005) 195003]

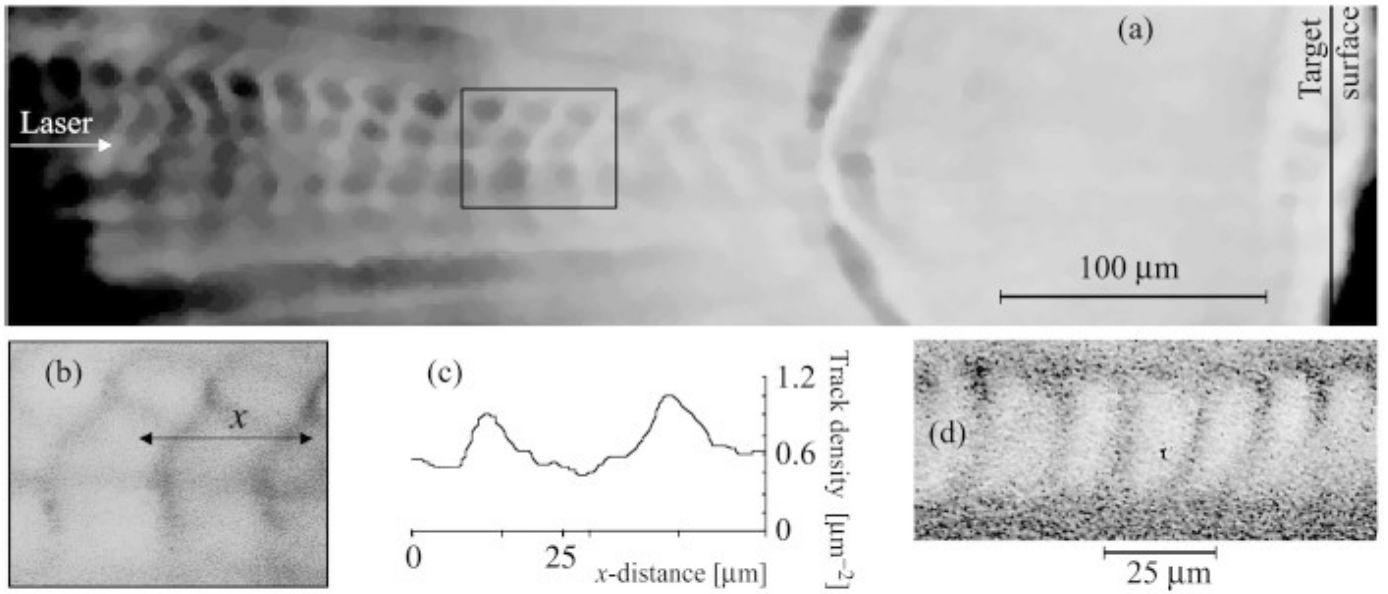

FIG. 1. (a) Proton projection image of the region in front of the laser-irradiated target, taken 20 ps after the interaction. The picture is a reflection scan of the exposed CR 39; (b) Detail of the image in frame (a), (c) Profile of the proton track density along the direction indicated by the arrow in (a); (d) Detail of the pattern observed at the back of a 0.9 μm Mylar target 20 ps after the interaction. The detail shown was located at a distance of about 200 μm from the original target plane.

Study of “coherent”, long-lived field structures

Theory and numerical simulations show that a variety of slowly varying structures (**solitons**, **vortices**, **cavitons** ...) is generated during laser-plasma interactions.

Regular, quasi-periodic structures observed inside or near the charge-displacement channel at late times

[T.V.Lyseikina, F.Ceccherini, F. Cornolti, E.Yu.Echkina, A.Macchi, F.Pegoraro, M.Borghesi, S.Kar, L.Romagnani, S.V.Bulanov, O.Willi, M.Galimberti, arXiv:physics/0701139]

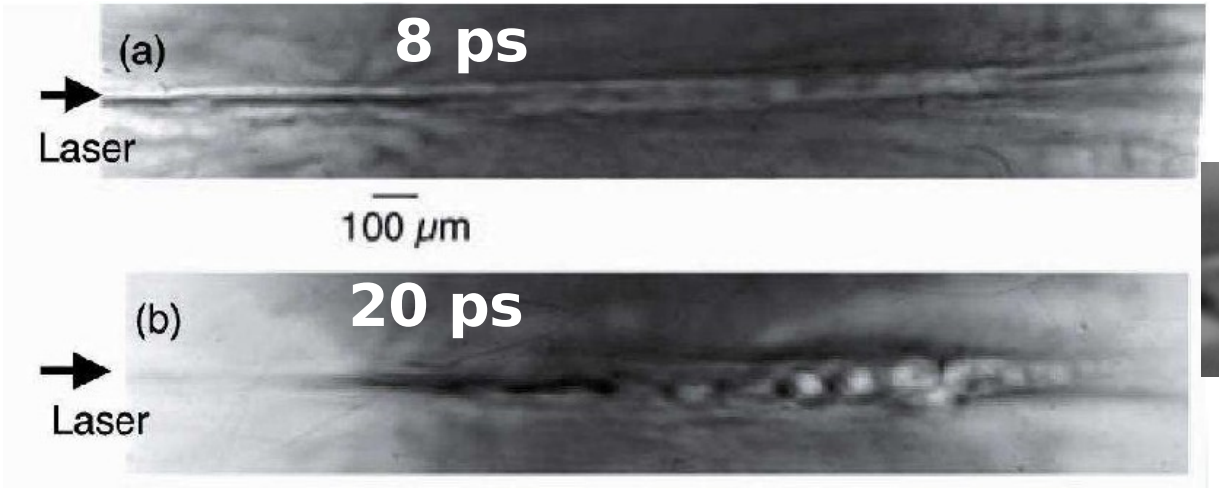

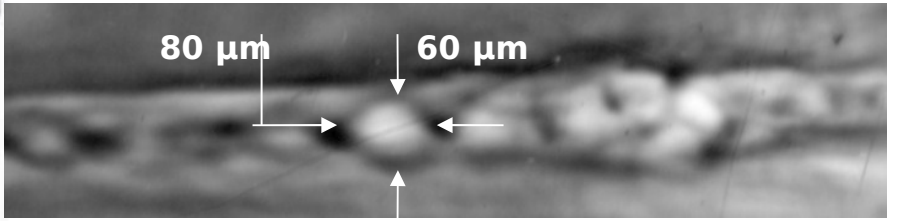

Coherent field structures in 2D PIC simulation

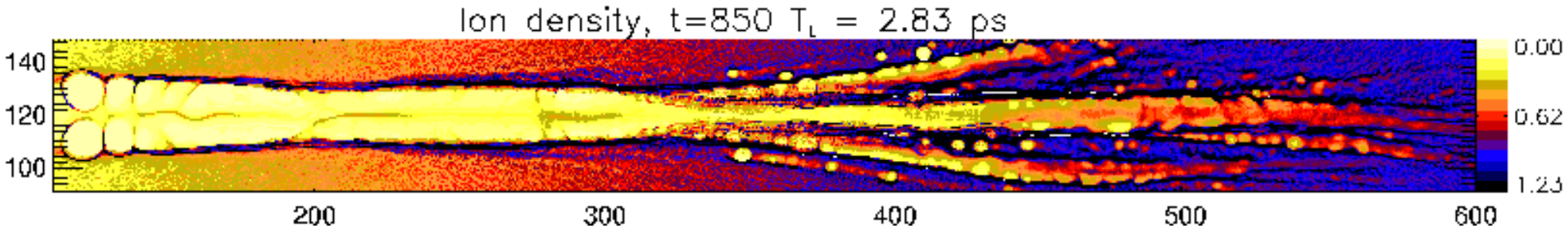

Pulse front: beam breakup and EM **cavitons**

Left channel side: "hybrid" quasi-periodic structures, "part **soliton**, part **vortex**"...

Lyseikina et al, arXiv:physics/0701139

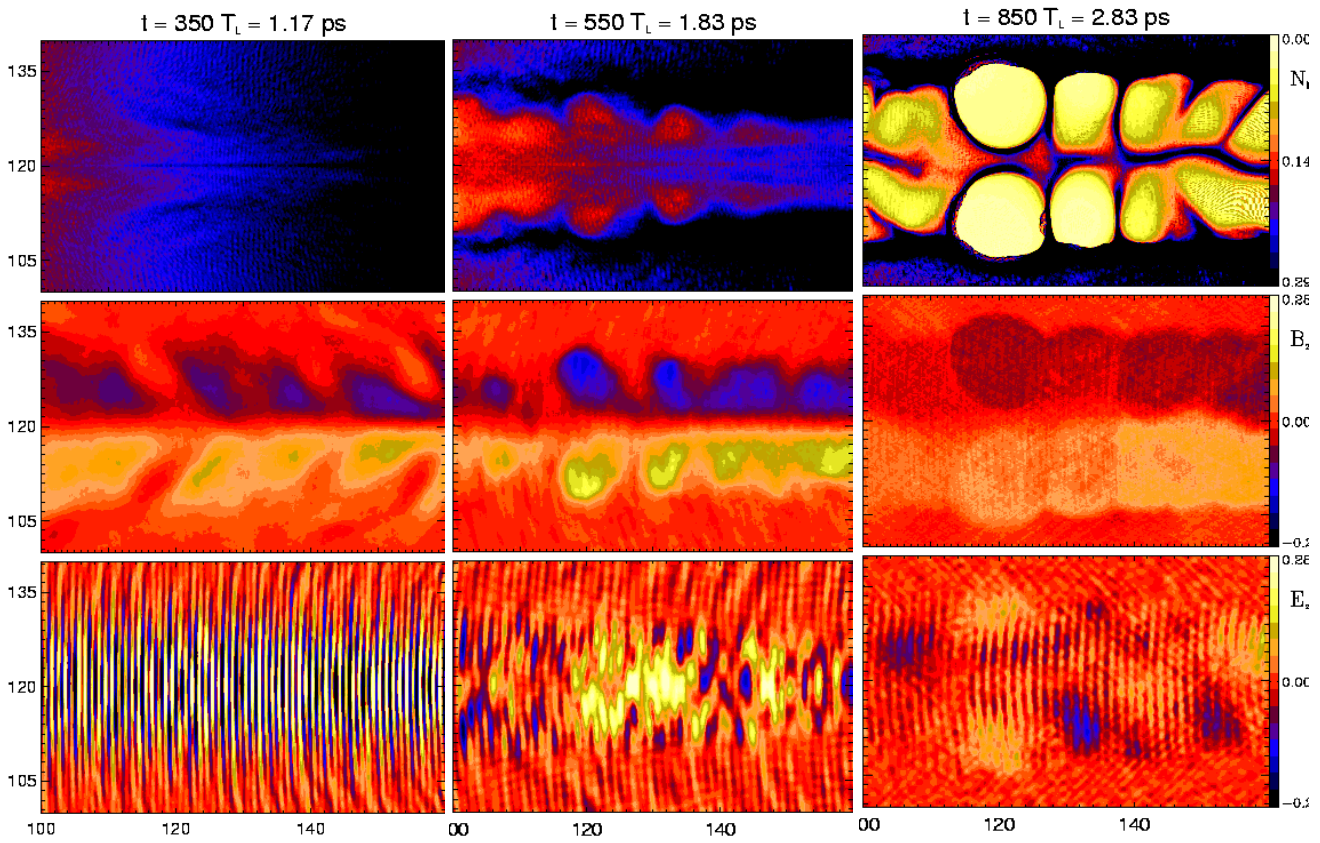

Conclusions

- The proton diagnostic technique offers for the first time the possibility to detect transient EM field in laser-plasma interaction

- Proton diagnostic data are challenging for theory and modelization

- Work is in progress for further developments and applications

  - multiple probe experiments?

  - magnetic field detection ?
    [see Li et al, PRL **97** (2006) 135003]

  - field inversion algorithms ?

This talk may be downloaded from

www.df.unipi.it/~macchi/talks.html

Chirped Pulse Amplification (CPA) technique

CPA concept: stretch the pulse in time by dispersion (chirping) to reduce power below the amplifier damage threshold

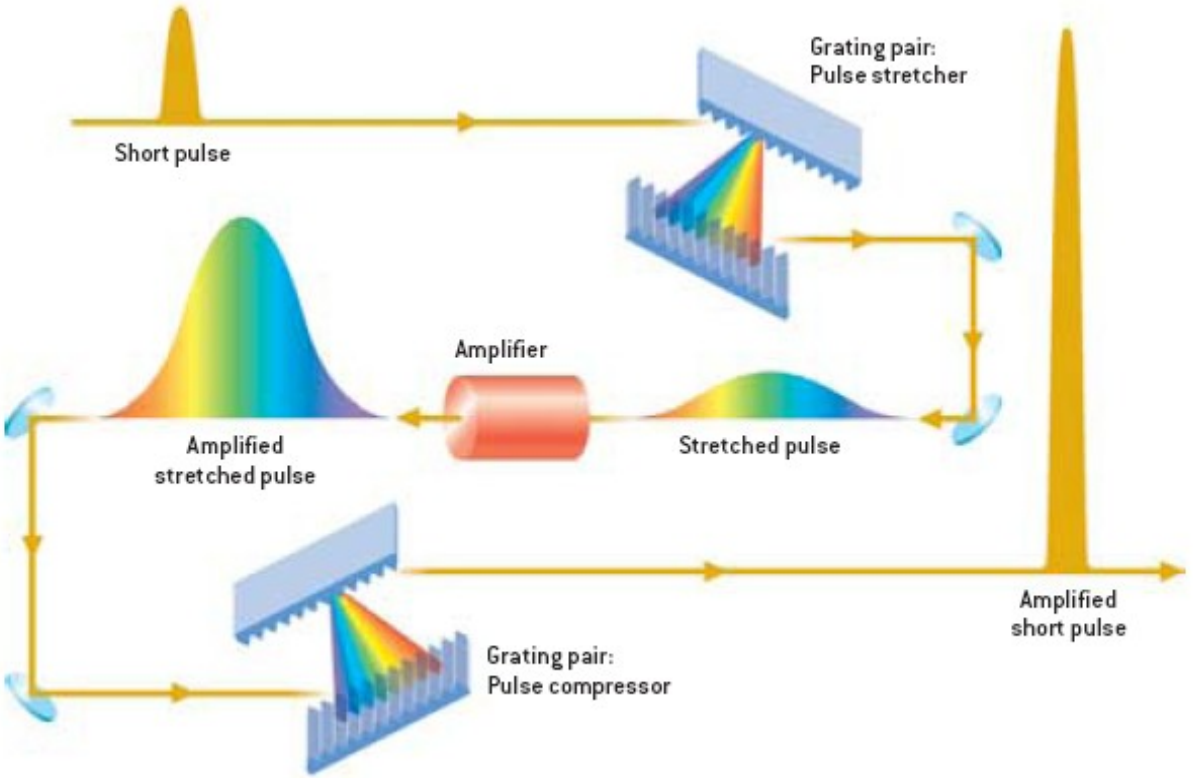

Donna Strickland & Gérard Mourou, Optics Communication (1985)

[Figure from: G. Mourou and D. Umstadter, Scientific American, May 2002, p.80]

On the origin of “fast” electrons

Forced oscillations of electrons across a sharp plasma interface ($L << \lambda$) are strongly non-adiabatic and lead to energy absorption from the EM (laser) wave

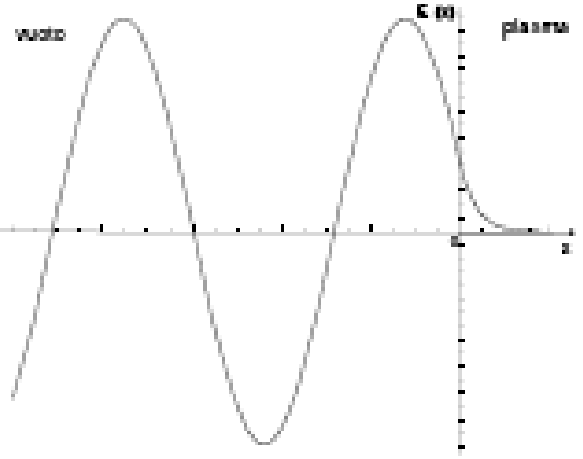

As can be shown with a simple electrostatic model at each cycle electron bunches are ejected into the vacuum region and re-enter the plasma with high momentum

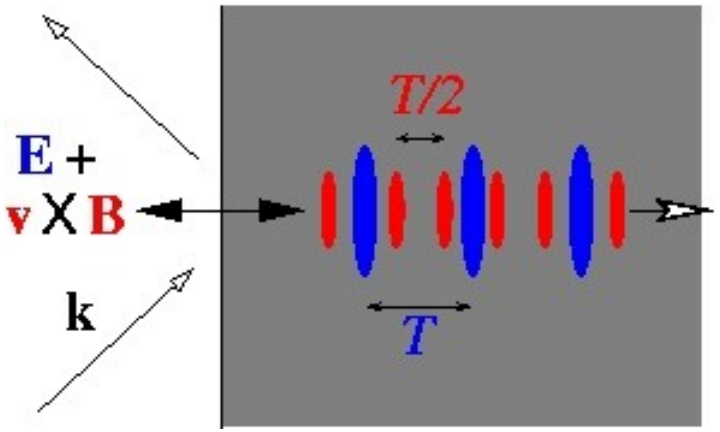

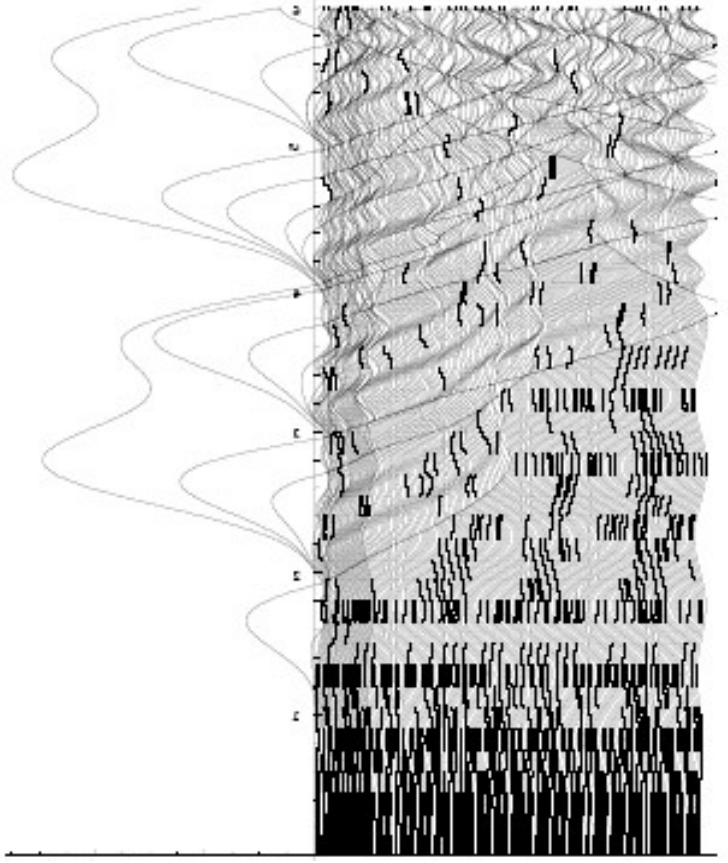

S. Tuveri, thesis, 2006

The $\mathbf{E}_{\perp}$ and **v**X**B** components drive electron bunches with different periodicity ($T=2\pi/\omega$ and $T/2$)

Basis of theoretical and numerical modeling

"Plasma physics is just waiting for bigger computers"

Vlasov-Maxwell system for *collisionless, classical* plasmas: kinetic equations are coupled to EM fields

$$\frac{df_a}{dt}(\mathbf{x},\mathbf{p},t) = \frac{\partial f_a}{\partial t} + \dot{\mathbf{x}}_a \frac{\partial f_a}{\partial \mathbf{x}} + \dot{\mathbf{p}}_a \frac{\partial f_a}{\partial \mathbf{p}} = 0, \quad a = (e,i)$$

$$\dot{\mathbf{p}}_a = q_a(\mathbf{E} + \mathbf{v}\times\mathbf{B}), \qquad \dot{\mathbf{x}}_a = \frac{\mathbf{p}_a}{m_a\gamma_a},$$

$$\rho(\mathbf{x},t) = \sum_{a=e,i} q_a \int d^3p f_a, \qquad \mathbf{J}(\mathbf{x},t) = \sum_{a=e,i} q_a \int d^3p \mathbf{v} f_a,$$

$$\boldsymbol{\nabla}\cdot\mathbf{E} = \rho, \qquad \boldsymbol{\nabla}\cdot\mathbf{B} = 0, \qquad \boldsymbol{\nabla}\times\mathbf{E} = -\partial_t\mathbf{B}, \qquad \boldsymbol{\nabla}\times\mathbf{B} = \mathbf{J} + \partial_t\mathbf{E}$$

Mostly used numerical approach: particle-in-cell (PIC) method
[Birdsall & Langdon, *Plasma Physics via Computer Simulation* (IOP, 1991)]

3D numerical simulations of "realistic" experimental conditions is most of the times beyond present-day supercomputing power

Models are needed to interpretate experiments and unfold the underlying physics